Nature. Author manuscript; available in PMC 2021 May 13.

Published in final edited form as:
Nature. 2020 November 01; 587(7834): 455–459. doi:10.1038/s41586-020-2866-8.

Enteric neurons increase maternal food intake during reproduction

Dafni Hadjieconomou[1,2], **George King**[1,2], **Pedro Gaspar**[1,2], **Alessandro Mineo**[1,2], **Laura Blackie**[1,2], **Tomotsune Ameku**[1,2], **Chris Studd**[1,2], **Alex de Mendoza**[3,4,5], **Fengqiu Diao**[6], **Benjamin H. White**[6], **Andre E.X. Brown**[1,2], **Pierre-Yves Plaçais**[7], **Thomas Préat**[7], **Irene Miguel-Aliaga**[1,2]

[1]MRC London Institute of Medical Sciences, Imperial College London, Hammersmith Campus, Du Cane Road, London W12 0NN, UK

[2]Faculty of Medicine, Imperial College London, Hammersmith Campus, Du Cane Road, London W12 0NN, UK

[3]Australian Research Council Centre of Excellence in Plant Energy Biology, School of Molecular Sciences, The University of Western Australia, Perth, WA, 6009, Australia

[4]Harry Perkins Institute of Medical Research, Perth, WA, 6009, Australia

[5]Queen Mary University of London, School of Biological and Chemical Sciences, Mile End Road, E1 4NS, London, UK

[6]Laboratory of Molecular Biology, National Institute of Mental Health, National Institutes of Health, Bethesda, United States

[7]Genes and Dynamics of Memory Systems, Brain Plasticity Unit, CNRS, ESPCI Paris, PSL Research University, 10 rue Vauquelin, 75005 Paris, France

Abstract

Reproduction induces increased food intake across females of many animal species[1–4], providing a physiologically relevant paradigm for exploration of appetite regulation. Parsing enteric neuronal diversity in *Drosophila*, we identify a key role for gut-innervating neurons with sex- and reproductive state-specific activity in sustaining the increased food intake of mothers during reproduction. Steroid and enteroendocrine hormones functionally remodel these neurons, leading

Author contribution statement

D.H. and I.M.-A. designed and conceived the study. D.H. and G.K. performed most experiments and analysed data. P.G. conducted crop enlargement, feeding and fecundity experiments, developed ways to quantify crop enlargement and analysed data. A.M. conducted some immunohistochemistry and fecundity experiments. L.B. conducted immunohistochemistry experiments and acquired and analysed feeding/crop enlargement videos. T.A. conducted some immunohistochemistry and RT-qPCR experiments. C.S. assisted with fecundity experiments, fly husbandry and video recordings. A.d M. performed phylogenetic analyses. F.D. and B.H.W. contributed the *Ms*^{TGEM}*-Gal4* mutant/driver line. A.B. provided the mathematical model. P-Y.P. and T.P. hosted and trained D.H. to perform *in vivo* brain calcium imaging experiments, P-Y.P performed calcium imaging experiments and analysed these data. I.M-A. wrote the manuscript, with contributions from D.H.

Competing interests

The authors declare no competing interests.

Europe PMC Funders Author Manuscripts

to post-mating release of their neuropeptide onto the muscles of the crop: a stomach-like organ. Post-mating neuropeptide release changes the dynamics of crop enlargement, resulting in increased food intake. Preventing enteric neuron remodelling blunts reproductive hyperphagia and reduces reproductive fitness. Thus, plasticity of enteric neurons is key to reproductive success. Our findings provide a new mechanism to attain the positive energy balance that sustains gestation which, if dysregulated, could contribute to infertility or weight gain.

Internal state has profound effects on brain function[5–7]. Despite increasingly recognised roles for the gut-brain axis in maintaining energy balance[8–13], links between internal state and gastrointestinal innervation remain poorly characterised. Progress has been hindered by neuroanatomical complexity, which is only beginning to be parsed in mammals[8,14–18]. The simpler –yet physiologically complex– *Drosophila* intestine provides an alternative entry point into the study of gastrointestinal innervation.

Innervation of the stomach-like crop

Innervation of the main digestive portion of the adult fly intestine, encompassing the anterior midgut and the crop[19,20] (Extended Data Fig. 1a,b), emanates from an enteric hypocerebral ganglion (HCG) (Extended Data Fig. 1c,e,g,i,j) and central neurons of the brain's *pars intercerebralis* (PI) (Extended Data Fig. 1a,d,f,g). PI neurons directly innervate the anterior midgut and crop, and include insulin-producing neurons[21–23] and other peptidergic subtypes[24] (Extended Data Fig. 1a,d,f,g). The crop is further populated by processes emanating from *corpora cardiaca* cells, which produce glucagon-like adipokinetic hormone and are adjacent to the HCG (Extended Data Fig. 1h; refs. [25,26]). Also adjacent to both the HCG and *corpora cardiaca* are the juvenile hormone-producing *corpus allatum* cells, which extend short local projections (Extended Data Fig. 1c,k). The thoracico-abdominal ganglion of the central nervous system may not innervate these gut regions (Extended Data Fig. 1l,m).

The crop (an expandable structure found in insect intestines[20]) might be disregarded as a passive food store, but several observations point to its active regulation. Refeeding flies following starvation resulted in enlarged, food-filled crops[27] (Extended Data Fig. 2a,d-e″), suggesting modulation of food ingression into/out of the crop. Live imaging or temporal dissections of flies revealed that food always enters the crop before proceeding to the midgut (Extended Data Fig. 2b-c'; Supplementary Video 1). Lastly, food transit through the crop is dependent on both its palatability and nutritional value (Extended Data Fig. 2f).

Thus, all food transits through the adult crop, which is nutrient-sensitive and shows chemically and anatomically diverse innervation.

Myosuppressin neuron control of the crop

The crop and anterior midgut are innervated by Myosuppressin (Ms)-positive neurons[28,29] located in the PI and HCG (Extended Data Fig. 3a,b,f,i-i″,o-o″). PI Ms neurons are distinct from known neuronal subsets, with the exception of 8 Ms neurons that co-express the *Taotie-Gal4* marker (Extended Data Fig. 3l-n″,p-q″). Two PI Ms neuron populations can be distinguished by size: ~ 18 large cells (including the *Taotie*-positive subset) and 12 smaller

cells (Extended Data Fig. 3i-i″). Single-cell clones of large Ms neurons reveal a single process that bifurcates into a longer axonal projection to the gut (which arborises in the HCG and extends further to innervate the crop) and a shorter, likely dendritic process that reaches the suboesophageal zone, where the axons of peripheral gustatory sensory neurons terminate (Extended Data Fig. 3c-e). A subset of HCG Ms-expressing neurons also innervates the crop, whereas another subset projects locally (Extended Data Fig. 3b and inset, respectively). We validated Ms expression using an endogenously tagged Ms reporter (Ms^{GFP}, see Methods) and *in situ* hybridisation (Extended Data Fig. 3j-k'). We also observed Ms innervation of the hindgut, rectal ampulla and heart, and a subset of peripheral Ms-positive neurons innervating the female reproductive tract (Extended Data Fig. 3f-h; data not shown).

We selectively activated or silenced Ms neurons in adult flies. Activation resulted in greatly enlarged crops in *ad libitum*-fed flies, consistent with the relaxant properties of Ms on insect muscles *ex vivo* [29,30] (Fig. 1a-a″; Extended Data Fig. 4b,d-d″). By contrast, silencing of Ms neurons prevented crop enlargement in a starved-refed situation (Extended Data Fig. 2a) in which the crop normally expands (Fig. 1b-b″; Extended Data Fig. 4c). Genetic downregulation or mutation of *Ms* (using a new mutant, see Methods) prevented crop enlargement, albeit to a lesser degree than Ms neuron silencing (Fig. 1d; Extended Data Fig. 4a-a″,e-e″,f-i). This could be due to another Ms neuron-derived neurotransmitter/neuropeptide contributing to crop enlargement, or to loss of Ms peptide during development in these experiments, resulting in adaptations rendering the crop more active than it would be in response to acute Ms peptide loss. We generated a *Gal4* insertion into the *Ms* locus that disrupts Ms production (Ms^{TGEM}; see Methods). In contrast to the crop enlargement resulting from TrpA1-mediated activation from *Ms-Gal4*, TrpA1 expression from this (*Ms* mutant) Ms^{TGEM}*-Gal4* driver failed to induce crop enlargement (Extended Data Fig. 4j,k), further confirming an *Ms* requirement. Neuron subtype-specific *Ms* downregulations and activations allowed us to establish that the PI Ms neurons (in particular, the *Taotie-Gal4*-positive subset of large PI Ms neurons) induce and are indispensable for crop enlargement through their production of Ms neuropeptide (Fig. 1d; Extended Data Fig. 4l,m).

We then explored contributions of Myosuppressin receptors 1 and 2 (MsR1 and MsR2)[31] (Fig. 1e). We observed *MsR1* expression in crop muscles, in subsets of neurons including the PI and HCG Ms-positive neurons and neurons innervating the ovary and heart (no *MsR1* expression was detected in ovarian/heart muscles) (Extended Data Fig. 5a-i'). Expression of *MsR2* was also detected in crop muscles (Extended Data 5i,i″). To investigate Ms receptor function, we downregulated *MsR1* specifically in adult crop muscles using two independent driver lines (*vm-Gal4* and $MsR1^{crop}$*-Gal4*, see legends for details). Both reduced crop enlargement in a starvation-refeeding assay, comparable to Ms silencing (Fig. 1c-c″; Extended Data Fig. 5k-o″). *MsR2* downregulation did not affect crop enlargement (Extended Data Fig. 5p). A role for *MsR1* in mediating crop enlargement was confirmed using a $MsR1^{TGEM}$ mutant (see Methods; Extended Data Fig. 5q-s). Thus, MsR1 is the crop muscle receptor through which Ms signals to modulate crop enlargement.

Neuron remodelling during reproduction

We next explored the physiological regulation of crop enlargement, and found that it is dependent on sex and reproductive status; crops of *ad libitum*-fed mated females (used for all the experiments described above) were consistently more expanded than those of *ad libitum*-fed virgin female or mated male flies (Fig. 2a-a″; Extended Data Fig. 6o). Since we failed to observe post-mating changes in Ms neuron projections (Extended Data Fig. 6a, b), we hypothesised that post-mating crop enlargement may result from preferential Ms release in mated females. Ms peptide in PI neuron cell bodies was lower in females only after mating in the absence of transcriptional changes (Fig. 2b-b″; Extended Data Fig. 6c,i), consistent with a post-mating increase in Ms peptide secretion in females. This effect was specific to mating: nutrient availability failed to affect Ms levels (Extended Data Fig. 6d-h). We also observed that the Ms neurons of mated females had higher cumulative calcium levels and reduced calcium oscillations than those of virgin females, as detected by both *in vivo* GCaMP6 calcium imaging and the calcium-sensitive reporter CaLexA (in which GFP expression is proportional to cumulative neuronal activity) (Fig. 2c,d; Extended Data Fig. 6j-n). Physiologically, and in contrast to mated females, reducing Ms signalling in males or virgin female flies failed to impair crop enlargement. Consequently, when Ms signalling to crop muscles was prevented, the size of the crop of mated females no longer differed from that of virgin females (Extended Data Fig. 6p,q). Collectively, these findings support the idea that, in females, mating changes the activity of PI Ms neurons to promote Ms release.

The steroid hormone ecdysone promotes egg production and is elevated post-mating[32,33]. The ecdysone receptor (EcR) is expressed by all PI Ms neurons (Extended Data Fig. 7a,a', 8i), suggesting that they may be sensitive to circulating ecdysone. Adult- and Ms-neuron confined expression of a dominant-negative EcR receptor (which targets all EcR isoforms) or *EcR* downregulation (using RNAi lines that target all isoforms or the B1 isoform specifically; see Methods) was found to increase intracellular Ms levels to virgin-like levels in the Ms neuron cell bodies of mated females, whereas they had no effect in virgin females (Fig. 3a-a″; Extended Data Fig. 7b-d). They also increased the amplitude of *in vivo* calcium oscillations in Ms neurons to virgin-like levels (Extended Data Fig. 8n,o). Compromising EcR signalling in adult Ms neurons significantly reduced crop enlargement preferentially in mated females (Fig. 3b-b″; Extended Data Fig. 7e-j): a phenotype also apparent when the PI Ms neurons were targeted using *Taotie-Gal4* (Extended Data Fig. 9k,l). Hence, ecdysone communicates mating status to Ms neurons through its B1 receptor.

We previously showed that mating resizes and metabolically remodels the adult intestine[34], but did not investigate effects on its hormone-producing enteroendocrine cells. We now observe a post-mating increase in enteroendocrine cell number, including a subset expressing Bursicon alpha hormone (Burs, shown to signal to adipose tissue via an unidentified neuronal relay[35]) (Fig. 3c-d; Extended Data Fig. 8a-c). An endogenous protein reporter for the Burs receptor Rickets (Rk/Lgr2) revealed expression in subsets of neurons including all PI Ms neurons (including the *Taotie-Gal4*-positive subset) and projections terminating in the HCG (Extended Data Fig. 8d-j′; expression in a subset of the HCG Ms neurons was observed only sporadically, Extended Data Fig. 8e).

Consistent with regulation of Ms neurons by the post-mating increase in enteroendocrine cell-derived Burs, adult-specific downregulation of its receptor *rk* in Ms neurons reverted Ms levels to virgin-like levels in the Ms neuron cell bodies of mated females, whereas it had no effect in virgin females (Fig. 3e-e″; Extended Data Fig. 8k-m). Like *EcR* downregulation, *rk* downregulation in Ms neurons also increased the amplitude of *in vivo* calcium oscillations in the Ms neuron cell bodies of mated females to virgin-like levels (Extended Data Fig. 8n,o). Functionally, both *Burs* downregulation in intestinal enteroendocrine cells as well as adult-specific *rk* downregulation in Ms neurons (either in all of them or in the *Taotie-Gal4*-positive subset in the PI) preferentially reduced crop enlargement in mated females (Fig. 3f-f″; Extended Data Fig. 9a-e,k,l). Conversely, stimulating intestinal release of enteroendocrine hormones including Burs from enteroendocrine cells resulted in reduced, mated-like Ms levels in the Ms neuron cell bodies of virgin females (Extended Data Fig. 9f-h), and greatly enlarged crops (Extended Data Fig. 9i-j) (see also Extended Data Fig. 8a'-a‴ for co-expression of *Tkg-Gal4* enteroendocrine cell driver and Burs).

Thus, steroid and enteroendocrine hormones communicate mating status to the brain. Acting through their receptors in the PI Ms neurons, these hormones change Ms neuronal activity, promoting Ms release after mating (Extended Data Fig. 9m).

Neuron remodelling promotes food intake

To investigate the significance of post-mating Ms neuron modulation, we selectively prevented crop enlargement post-mating by downregulating *MsR1* in adult crop muscles using two independent strategies (Extended Data Fig. 5k,l). This did not affect males or virgin females, but specifically prevented the increase in food intake normally observed in female flies after mating[1] (Fig. 4a,b; Extended Data Fig. 10a-e). Comparable results were obtained by blocking the post-mating ecdysone and Burs inputs into the Ms neurons (Fig. 4c,d; Extended Data Fig. 10f,g). *MsR2* downregulation had no such effect (Extended Data Fig. 10d). Thus, the post-mating change in crop expandability mediated by Ms/MsR1 signalling causes the increased food intake observed in females after mating.

The negative pressures reported in crops of larger insects[36] suggest that the crop may draw food in by generating suction. The increased crop expandability enabled by post-mating Ms release could therefore increase food intake through changes in suction. We observed that mated females ingest more food per sip than virgin females (see Source Data), consistent with mated females needing to generate a higher suction pressure to facilitate bigger sips. We therefore modelled crop enlargement using the Poiseuille equation for incompressible fluid flow in a pipe (see Methods), and found that the crop would need a suction pressure on the order of -1kPa to achieve the intake volume previously reported per sip[37]. This is in reasonable agreement with previously reported values measured in cockroach crops of between -0.5 and -1kPa[36]. The model predicts that mated flies would require a modest increase in suction pressure to -1.3kPa to facilitate the increased sip size.

In the model, crop volume change drives food intake via increased suction (Extended Data Fig. 10h). Hence, a crop that cannot enlarge or a persistently enlarged crop should both result in a comparable reduction in food intake by preventing suction generation. We tested

this by persistently preventing crop enlargement (using crop muscle-specific *MsR1* knockdown, Extended Data Fig. 5k,l), or by persistently inducing it (using TrpA1-mediated Ms neuron activation from *Ms-Gal4* or *Taotie-Gal4*, Extended Data Fig. 4l,m), after which we assessed food intake by switching flies from undyed to dye-laced food. Both genetic manipulations indeed reduced intake of the dye-laced food (Extended Data Fig. 10d,e,i,j,m). Conversely, increasing the rate at which the crop expands should increase food intake. We tested this by activating the Ms neurons as in the previous experiment, but this time we switched the flies to dye-laced food and monitored their intake at the same time as we activated the neurons (i.e. as we were inducing greater crop expansion) rather than after a persistent activation (when the crop is already maximally expanded). We observed increased food intake in these conditions (Extended Data Fig. 10k,l,n). Although further work will be required to elucidate the full dynamics of crop enlargement, filling and emptying, these experiments support the idea that the Ms-induced post-mating enlargement of the crop increases food intake at least partly through increasing the crop's suction power.

Finally, given the links between nutrient intake and fecundity[38], we hypothesised that the Ms-driven post-mating crop enlargement may be adaptive and support reproduction. Selectively preventing crop enlargement post-mating by downregulating *MsR1* as previously described reduced egg production (Fig. 4e; Extended Data Fig. 10o). Eggs that were produced also showed reduced viability (Extended Data Fig. 10p). Thus, the crop and its Ms innervation help sustain the post-mating increase in food intake, maximising female fecundity.

Discussion

Our findings lead us to propose that the maternal increase in food intake during reproduction is adaptive, the crop is a key reproductive organ, and Ms a major effector of post-mating responses. In support of these ideas, the crop is absent in larvae –the juvenile stage of insects–and other Diptera have co-opted it for reproductive behaviours such as regurgitation of nuptial gifts or secretion of male pheromones[20]. Ms receptors are also closely related to the Sex peptide receptor (the "mating sensor" of female flies), and both diverged following duplication of an ancestral receptor which might have responded to the Myoinhibitory peptide (Mip) in the last common ancestor of protostomes[39]. It will be interesting to explore possible links between Ms and Sex peptide signalling.

We provide evidence for a *Drosophila* gut-to-brain axis by identifying central Ms neurons as targets of a gut-derived hormone: Burs. These central neurons innervate the gut, "closing" a gut-brain-gut loop that connects midgut enteroendocrine signals to the crop: a more anterior gut region. This may allow functional coordination of different gut portions, whilst enabling central modulation by sensory cues (e.g. gustatory). We also identify the Ms neurons as the neural targets of ecdysone, shown to promote food intake[40]. Reproduction has significant and lasting effects on the human female brain[41,42]; Ms neurons provide a tractable and physiologically relevant neural substrate to investigate the mechanisms involved.

Our own digestive system may be similarly modulated by reproductive cues to affect food intake. In mammals, enteric neurons express sex/reproductive hormone receptors[43] and

enteroendocrine hormone levels change during reproduction[3]. We argue that pregnancy and lactation represent an attractive, relatively unexplored physiological adaptation to investigate mechanisms of nutrient intake regulation, organ remodelling and metabolic plasticity: mechanisms that might eventually be leveraged to curb appetite and/or weight gain.

Methods

Fly husbandry

Fly stocks were reared on a standard cornmeal/agar diet (6.65% cornmeal, 7.1% dextrose, 5% yeast, 0.66% agar supplemented with 2.2% nipagin and 3.4% propionic acid). All experimental flies were kept in incubators at 65% humidity and on a 12h light/dark cycle, at 18°C, 25°C or 29°C depending on the specific experiment. Flies were transferred to fresh vials every 3 days, and fly density was kept to a maximum of 20 flies per vial. 4-day and 7-day-old virgin flies were used for experiments at 18°C and 25°C, respectively, unless otherwise indicated.

Temperature-controlled experiments—We used *UAS-TrpA1* to activate Ms neurons (neuropeptide release) and to force release of peptides (including Burs) from enteroendocrine cells. For pre-activation of Ms neurons to assess crop enlargement/feeding, we transferred flies to a 29°C incubator for 4h prior to transfer to dye-laced food. For concurrent activation of Ms neurons during feeding, flies were transferred to a 29°C incubator at the same time as they were transferred to dye-laced food (to allow crop expansion during feeding before it reaches maximum size, Extended Data Fig. 10k,l,n). In starved-refed scenarios, feeding was monitored over the course of 15-20min; in fed *ad libitum* conditions, feeding was monitored over the course of 2h (or for 1h when comparing pre-activation with concurrent activation of Ms neurons with feeding). To force enteroendocrine peptide release we extended the incubation at 29°C to 14-16h. For Ms neuron silencing (neuropeptide retention) we used the ubiquitously expressed temperature sensitive Gal80 allele (*tub-Gal80^{TS}*) recombined with the *UAS-kir2.1* transgene. Flies were reared, aged and mated at 18°C. They were then transferred for 24h at 29°C and either starved or kept feeding *ad libitum* for an additional 14-16h at 29°C. Next, experimental assays were carried out at 29°C.

RNAi experiments were also performed at 29°C unless otherwise indicated. For these, flies were reared and aged at permissive temperature (18°C) and then transferred to 29°C for RNAi induction for 5 days. Experimental assays were carried out at 29°C.

Ms-Gal4 Flybow clones were generated using the Flybow 1.1 construct based on the method described in[44]. A multiple heat-shock approach at different developmental timepoints was used. Each heat-shock lasted 1h at 37°C.

Diets

For experiments exploring the dietary regulation of crop enlargement, we used agar-based diets with a single nutrient source supplemented with 1% E133 Duracol brilliant blue FCF (Sigma, 807171, referred to as FCF blue). The basic recipe contained 1% agar, 1% FCF blue, 2.2% nipagin and 3.4% propionic acid. Each specific nutrient was added to the basic

recipe in the following amounts: sorbitol only 18.2% (1M), yeast only 5%, arabinose only 15% (1M) and sucrose only 34.2% (1M). For details of these diets and their palatability/nutritional value see[45–47]. Times displayed in Extended Data Fig. 2b-b‴ panels correspond to times after initiation of feeding of the dye-laced diets; only flies that continued to engage with the food following initiation of feeding were dissected and scored.

To assess the effect of starvation on Ms levels, 4-5 day-old virgin female flies or female flies mated for 24h were placed on 1% agar for 16h prior to immunohistochemical analysis.

For fecundity assays, which required daily egg counting, experimental flies were kept in cages on apple juice plates with a smear of live yeast. Plates were changed every 24h.

Refeeding assays required visualization and/or quantitation of food in the fly gut. For these, 1% FCF blue was added to the standard fly food. When pre-starvation was required, flies were kept in vials containing 1% agar in Milli-Q water, with 2.2% nipagin and 0.34% propionic acid.

FlyPAD food was pan-cooked using 1% agarose, 5% live yeast (*S. cerevisiae*) and 7.1% dextrose. It was dispensed into 2mL Eppendorf tubes and stored at -20°C until used. The food was melted to liquid form using a heat-block at 95°C. It was then dispensed as a viscous droplet in the flyPAD set up, where it fully solidified.

Fly stocks

Drivers— *nSyb-Gal4* (original insert on 3rd chromosome, gift from Julie Simpson), *Ilp2-3-Gal4* (ref. [48]), *Gr43a^{KI}-Gal4* (ref. [49]), *Dh44-Gal4* (ref. [50]), *Mip-Gal4* (ref. [51]), *pain-Gal4* (ref. [52]), *Gr28a-Gal4* (ref. [53]), *Aug21-Gal4* (BDSC: 30137), *Ubx-Gal4* (ref. [54]), *abd-A-Gal4* (ref. [55]), *Ms-Gal4* (ref. [56]), *Taotie-Gal4* (ref. [57]), *Dsk-Gal4* (ref. [56]), *MsR1^{TGEM}-Gal4* (this study), *vm-Gal4* (ref. [58]), *rk^{TGEM}-Gal4* (ref. [59]), *voila-Gal4* (ref. [60], stock combined with *tub-Gal80^{TS}* was a gift from Julia Cordero), *Tkg-Gal4* [61], *tub-Gal80^{TS}* [62], *nsyb-Gal80* (ref. [63], gift from Julie Simpson).

Reporters—Ms^{GFP} (this study), *UAS-FB1.1* (ref. [44]), *UAS-DenMark-RFP, UAS-Venus-pm* (ref. [64,65], recombinant was a gift from Matthias Landgraf), *UAS-hs-mFlp5* (ref. [44]), *UAS-TrpA1* (ref. [66]), *UAS-Kir2.1 (ref.* [67]), *UAS-Ms-RNAi* (VDRC: GD 4874), *UAS-Ms-RNAi* (TRiP: JF02144), *UAS-stingerGFP* (ref. [68]), *UAS-MsR1-RNAi* (VDRC: GD 9369), *UAS-MsR2-RNAi* (VDRC: GD 42304), *UAS-CaLexA* (ref. [69]), *UAS-GCaMP6f* ref. [70]), *UAS-EcR-RNAi^{97}* (BDSC: 9326, referred to as *EcR^{RNAi-1}*), *UAS-EcR.B1-RNAi* [168] (BDSC: 9329, referred to as *EcR^{RNAi-2}*), *UAS-EcR-RNAi* (VDRC: GD 37058, referred to as *EcR^{RNAi-3}*), *UAS-EcR^{DN}* (BDSC: 6872), *UAS-rk-RNAi* (VDRC: GD 29932*), UAS-dcr2* (VDRC: 60010), *UAS-Burs-RNAi* (VDRC: GD 3951).

Mutants— *MS$^{\Delta}$ (this study), Df(3R)Exel6199 (BL7678), MsR1^{TGEM}-Gal4* (this study), *Ms^{TGEM}-Gal4* (this study), *Df(3L)Aprt-32* (BDSC: 5411).

Oregon R (*OrR*) and *w* [1118] were used as control flies

Generation of Ms^{GFP} transgenic reporter line—The CBGtg9060F04101D GFP-tagged clone for Ms from the fosmid library TransgeneOme Resource (Source Bioscience[71]) was used to establish transgenic lines using φC-31 integrase mediated recombination (BestGene). The landing *attP* site used was *attp40*(*y* ^{1} *w* ^{67c23}; *P*{*CaryP*}*attP40*).

Generation of Ms^{Δ} null mutant— Ms^{Δ} was generated using CRISPR/cas9 assisted homologous recombination as described in ref. [72]. The entire coding region of the gene was removed and replaced with an *attP* site and an excisable Pax3-mCherry cassette. We chose to use a two-gRNA approach (gRNA1: 5'-TTTTAGAGCTAGAAATAG-3' and gRNA2: 5'-AACACCACTTGGTCCCGA-3'), making use of the *pCFD4* vector (Addgene #49411). The two homology arms were cloned in the modified *pTV3-mCherry* vector (gift from Cyrille Alexandre). Both vectors were injected into *yw; nos Cas9(II-attP40)* flies by BestGene.

5'-Homology arm : GTGCTTGCGTTCAACAAGTCCAGCAAACAGAGCAGCAGCTGAACCCCGGTGTTAACAACTAACAAGT

3' Homology arm : CCGACATGAGACAACGACACTGGACCCTGACCACAAGCGGCGGAATCGTTTCTGTTCACCCAAAAAG

Generation of Ms^{TGEM}-*Gal4* mutant/driver line

The Ms^{TGEM}-*Gal4* mutant line was made by inserting a Trojan Gal4 Expression Module (TGEM, ref. [73]) into a PAM site (GTAATTGATAAGTAATCTTGAGG) within intron 3 of the *Ms* gene using CRISPR/Cas9. To make the TGEM construct, homologous arms of approximately 700bp flanking the Cas9 cleavage sites were synthesised by Integrated DNA Technologies, Inc (Coralville, Iowa, USA) and were cloned into the *pT-GEM(1)* vector. The resulting *pT-GEM(1)-Ms* plasmid was co-injected with a *pBS-U6-sgRNA-Ms* plasmid encoding the guide RNA into embryos of flies expressing germline Cas9. Transformants were identified by their expression of the 3xP3-RFP marker.

5' homology arm—

ATTTCGAGCGTAATCATCATCCCGAGGCGTTGACGCAGAACAAATTGCCTTAGCCT
CCGCCATTTTCAGCTAATAGAAACAAATTGTGTGTCGCGTAAACGTATTAGGGTAC
CATTAAGACGCCTGCTTGGATGCGATTTAAAATGGTAACACCGCCGCTAGCCAGA
AGGCCAAGTACAACTCCATTTATGCATAATACTTTGCCAGGGCAACGCCATCATCA
GCGAATGGCAATCAGGCACGTAGCATTAAGATCATTACACTTAATCAAAATCAGTG
GGGTTGGATGGGCATGGGGCATGTAGCATGGAGCGTGGAGCTTGGCTTAGTCGCC
CTCCAGCCAGGATGTCCTTGCCGCGCAACCTTTGCCGGCGATAATCAAATAAGCT
CGACACCAGCTTTCGTTGTCAATCATGTTTCATAACCCACTTGCAGCATGTCCTTC
GCTCAGTTCTTTGTCGCCTGCTGCCTGGCCATCGTCCTCCTGGCCGTGTCCAACA
CACGGGCCGCAGTCCAGGGTCCACCTCTATGCCAGTCTGGCATCGTCGAGGAGAT
GCCCCCGCACATCCGGAAGGTGTGCCAGGCCCTGGAGAACTCCGATCAACTGAC
GTCGGCGCTGAAGTCCTACATCAACAACGAGGCATCCGGTGAGTGAATCAGGACC
AGAGAATTTACCT

Europe PMC Funders Author Manuscripts

3' homology arm—

TAAGATTACTTATAAATTACTATGCTTGCTCCAGCTTTGGTGGCCAACTCTGATGAC
CTGTTGAAGAACTACAACAAGCGAACGGATGTCGATCACGTCTTCCTGCGTTTCG
GAAAACGTCGTTAAGGACATTTTTTTGCAAGGACATCCCGAACACCACTTGGTCG
CGACATGAGACAACGACACTGGACCCTGACCACAAGCGGCGGAATCGTTTCTGTT
CACCCAAAAAGCACAACACTATTTTGACGTCTTCAGCATAATTATGTAAACGTAAT
CGATGGAAACTCAGAACTATACTCAATTGGAAGCTCTCTAGTTCATTAAATATCCA
ATGTCCAATGTTTCTATGCAACAAAAAAAAAATCGAATACATATTTGTAAATACTC
AAAGACCCTCGAAATGTTCTGAAAGTTAAACCCTTGGTTTTGATTTAATTCGTACT
CTTTATTTGCTGAGTGTTATAAAGAACTAATAATACGTATTTCAACGATGTTTAAATA
TCTCACACATATTTCCCTAGCATGAAGCACTATTATTAAATAACCAACAAATGTTTT
CAAATCCAAACACTATTTTCCGTTGTATACTTTAATAAAGACAAACTTTTCCTCTCA
ATTTGTGAATGCATAGCAAAATGCAATTGAAATGGTTTACATTTAATAGGAAAGTT
GGGCTACTCTTTGAACAA

Generation of *MsR1^{TGEM}-Gal4* mutant/driver line

MsR1^{TGEM}-Gal4 was generated using the method described in ref. [73]. The coding intron flanked by the first two coding exons of *MsR1* locus was targeted for double strand breaks by two different gRNA's (gRNA1: 5'-GGGCTCCAGGTGGGACGTAC-3' and gRNA2: 5'-GAGTCGGCAGAGGTCCGCGG-3'). Similar to *MS$^{\Delta}$*, a two-breaks approach was used to minimise off-target breaks, and the *pCFD4* plasmid (Addgene #49411) was used for gRNA expression. Homology arms flanking the *Cas9* cut sites were subcloned into the *pTGEM(1)* (Addgene #62893) plasmid. Both vectors were injected into *yw; nos Cas9(II-attP40)* flies by BestGene.

5'-Homology arm—

GGCAACATCATAGCCATTAGCTGCTGGCGCAAGGGAACCGTTCAAAAATCGATTA
TCGCCCCATTTCGGGGGAGCTTCTATTTTGATTTGCCGTACAATTTTCTCGGGCGA
TTAAACGACGAAGCAGAACGAAAACAAAAAACAGATTTGTCAACAGCAAGGTCA
ACAATTGATGGCTGAAATCAATTTAATTGACCATATCCTACGGGCCCTCCAAGTGG
CCATCTGCTGCACCTATAAAAAAGTGAATCCGGTCTGCGATTATTTATATATTCGTT
GCATGGCAGGCGGTCGTAAAACCTCGAGATGATGATTAAAAGCGGCCCTAAAAAC
TTAATGGCGGTTTAGGAAATTCAATTCCTGTAATTTAAGCCGAGTCACCATTCTTC
GAAGTTCTTACATGTAAGCGATAATAAATAGTTAAGTCAATTGGCCAATAAACCTAT
TAATATTGTGCATTTACCACGATTAGACTTTGATTAAAGTGACAATGCTGATTTCTG
TAGAGGAAATCTAGTTCTAGTCTTCCCACAAAGCTATTTAGTTACTCTTGAATAAAT
ATGTTACTTTTCTTTTGCCAAAACCAACAGAATTTTAAATTTAATAATTTGGATTTT
TTGCAATAAACTGTACTGATTAATGGGCCACACAAAAATGTCTAGTTTATTATGGA
GCTCTTGGTTTCATAAATTAAGAACATAATCCAATCGGCATATAAATCATTGATAGC
AATTTATTTTCCGTGATGAAACTGTGCTCCGTGTGAACTGCGAATTACTCATTCTAC
GGTTGCAAAAAAAGCCACCAACGGTCAACATTTAGACCAGGACTTTTAGTTTTAA
TTAGAGCCAGCCTGGCCAACAGCAGTGTTAATGACCACAAAGTGGCTGGCCACAG
GATCAGCATCCCAGAATGCGATGCCGCATTTGCTTTAATTAAAGGTAGTAGCTGGA
GTTTGAAAGATGACTGTATGGCAATTAGATGTGTAGCCAGAACACTTGGCCATTTA
CTTTTGTGTCAAAGTCGTGCCAAATTGCCAGCGGAGGCGACACTTGACGCTGTCA

Europe PMC Funders Author Manuscripts

CGCCCCAGACAGACGCAGACCGGCCCAAAAGCACCCACTCAGCCGTCTCCAGGC
GCCACTCAAGCGGCAAAGGAACGCCAAAACACTAGGACACAGAACGCCAGAAG
ACTCGAAAAAAAAGTAT

3' Homology arm—

CGGCAACGACAACAACGTCGACGACATGAATGAAGTCCTGGAATTGTTTTGCACC
AGGATGGCATCGGGGCTCCAGGTGGGACGTACTGGCTCAAAGTTATTGGCCCAGA
AATCAGGCATAGTTAGCTGCCGAAATGAAACCCAAATACCGAGAAAACTAGGCAA
AACAAACAGTAGTACACCGGAAATGCATATCATTGTAAAAACTACATCAGTTTACC
TAAAAGGCTTGGCTTTTAAGCTTTCACATTTATAAAATATTGAAAATGCATATAAAA
GTATGAAATTAATTCCCTTTTGTCAATAAACTTTCTTTCTTTCTTTCTGTGTAATATG
GGGGATACCGGTTTTTTTTTTTTTTCAATGAAATCCCTTCGAAAGGTATAAGTTCA
GAATCGAGAGTTTTATGCCAAGTTGGGCACAGTTTTTTTTTTCCCCAGCTACCTAA
AATAATAGAGACATTTTCCTCCCACTACAACTGATTGCATTGCCGGTGCAGAAAGT
TTTTTCAGTTGGTTCGGAAAAATTTGGTTCGCAAACAAATTAATATGAACTGGCAA
GCATTTTTCGGGCAAAAAGCTCTCATCTATGTAGATTGGAATGGAAATTCCGGCTA
GAATTGCATAAGACCACCTGCAGTGTGGGCTAACATGACTAAAAAGTTGTCCACA
AATTTGGCTTAGATTCTCCAATAAAACTGTCGTTCGGCCAGGAATCCCCTTTTTTG
TTTCGAGTGAATGGGGAATTTCGCACGACAGACAGCAATAAAGAATTTAACTAAA
GTCCTGACACCGACAGCACCAGCAGGACGCACACGTGTCACTCCATTTGGAGAGC
TTGGAGTATATTAAACATTTTTTCCCCACCAGTCAGCCGCAGGACTTGCATCGGTC
TCGCCTCGCATTTTCCTATATAAATTTTATGCTAAGTCTAATTTGTTGGCTGCAACTT
GCACAAAGGCAAAAAATAAACAAGGGCGAAATGCCGAAAGCCAAAACCCAACC
GAAACCGTTGAGGGCTGCCTCGCTTTTTTCCTGTGCCGAATTCCCTAAAACTTTG
CACATAAATTTGAGTCCTGCGCCTGGGCTTTTCCTCTTCCACCT

RT-qPCR

RNA was extracted from fly heads in groups of 20 flies using Trizol (Invitrogen). RNA was cleaned using RNAeasy mini Kit (QIAGEN), and cDNAs were synthesized using the QuantiTect-QIAGEN reverse transcription cDNA synthesis kit from 500ng of total RNA. Quantitative PCRs were performed by mixing cDNA samples (5ng) with TaqMan Master Mix (ThermoFisher, 4369016) and commercially available probes for *Ms* (ThermoFisher, 4351370 (Dm02152471_g1) and *aTub84B* as a control housekeeping gene (ThermoFisher, 4331182 (Dm02361072_s1). Three biological replicates were used for each sex/mating condition, and each biological replicate consisted of 20 pooled brains. Values were plotted as relative to *aTub84b* expression.

Sequence search and phylogenetic analysis

The *Drosophila melanogaster* MsR1 and MsR2 sequences belong to the Pfam domain 7TM_GPCR_Srw (PF10324). This domain was used to scan a reference panel of metazoan genomes covering the whole span of metazoan diversity using HMMER3[74]. Given that no sequences for deuterostomes were found using HMMER3, we then used BLASTP to search for MsR1-like amino acid sequences in vertebrate genomes. The resulting 294 sequences from both searches were aligned using MAFFT[75] linsi mode, then trimmed using trimAL[76]

in gappyout mode. The trimmed alignment was fed into IQ-TREE[77] using automated mode for model selection and 100 bootstrap replicates to compute nodal support. The resulting tree was rooted using vertebrate sequences as an outgroup.

To search for Sex Peptide, Ms and Mip, we blasted the *D. melanogaster* sequences against metazoan genomes and gathered the best hits of closely related species based on an e-value < 1e-05, aligned them using MAFFT, curated the alignment and used it to build a sequence profile for HMMER3[74]. These HMMER3 profiles were then used to scan the reference set of metazoan genomes with higher accuracy. Hits for distantly related species were inspected manually to avoid false positives and validated using the reciprocal best hit criterion against *D. melanogaster* genome.

GPCR phylogenetic tree

https://www.dropbox.com/s/3wre9qzy6i0uyyo/7TM_GPCR_Srw_phylogeny.tree?dl=0

GPCR sequence alignment

https://www.dropbox.com/s/ntb0nzx9jutanto/7TM_GPCR_Srw_phylogeny.al.fasta?dl=0

Software versions

MAFFT v7.221

trimAL v1.4.rev15

HMMER 3.1b2

IQ-TREE 1.5.5

Crop model

To model the effect of crop suction on food intake, we assumed that the oesophagus, crop duct, and gut are cylindrical tubes (providing some resistance to flow) and that the crop itself is a sphere that can expand and contract (Extended Data Fig. 10h). We then used the Hagen-Poiseuille equation to relate the measured dimensions of the digestive system to the hydraulic conductivity K in each branch, giving a flow rate $J = K\Delta P$ where ΔP is the pressure drop along the segment and

$$K = \frac{\pi r^4}{8\mu L},$$

where r is the radius, μ is the viscosity, and L the length. Assuming the gut valve is closed when the crop is expanding, $J_o = J_c = dV_c/dt$, the volume rate of change of the crop. If we further assume for simplicity that the pressure at the mouth is zero, we find the pressure in the crop

$$P_c = -\frac{dV}{dt}\left(\frac{1}{K_c} + \frac{1}{K_o}\right).$$

Higher flow rates require larger negative pressures in the crop, while higher conductivities mean the same flow can be achieved with smaller negative crop pressure. We measured the dimensions of the oesophagus and crop duct from microscopy images to estimate their conductivities, and the sip duration (0.13s) and intake per sip (1.05nL) were taken from ref. [37] to estimate *dV/dt* of the crop in mated flies. We calculate that the intake per sip for virgin females is less by a factor of 0.6 compared to mated females, based on our own quantifications of sip number and total food intake (see Source Data). The crop pressure required to achieve the measured flow rate from[37] is -1kPa which is comparable to the -0.5kPa to -1kPa measured in cockroach crops[36], suggesting that crop suction is a plausible physiological mechanism to drive food intake.

Immunohistochemistry and tissue stainings

Following dissection, the central and enteric nervous systems, gut-associated secretory glands together with intact intestinal tissues were fixed at room temperature for 45min in PBS, 4% paraformaldehyde. All subsequent washes were done in PBS, 4% horse serum, 0.3% Triton X-100 at room temperature following standard protocols. Primary antibody incubations were done at 4°C overnight, whereas secondary antibody incubations were done at room temperature for 2h.

The following primary antibodies were used: rabbit anti-Akh (ref. [25], 1/200), rabbit anti-Burs (ref. [78], 1/200), rat anti-Elav (DSHB, 7E8A10 1/25), mouse anti EcR (DSHB, DDA2.7 1/10), goat anti-GFP (Abcam, ab5450 1/1000), rat anti-Ilp2 (ref. [79], 1/500), rabbit anti-Ms (ref. [80], 1/1000), mouse anti-Pros (DSHB, MR1A 1/25).

Fluorescent secondary antibodies (FITC-, Cy3- and Cy5-conjugated) were obtained from Jackson Immunoresearch and used at 1/200. Vectashield with DAPI (Vector Labs) was used to stain DNA. Phalloidin stainings were performed after immunohistochemistry using mushroom phalloidin AlexFluor®647 probe (Life Technologies #A22287, 1/200 for 45min).

Custom-made fluorescence *in situ* hybridisation probes were outsourced to either Stellaris RNA FISH (for *Ms* transcript) or Advanced Cell Diagnostics RNAscope (for *MsR* and *Rk* transcripts). Dissection tools and surfaces were treated with RNaseZAP™ for single RNA *in situ* stainings, which were generally conducted according to the standard manufacturer's protocol following tissue dissection. For Stellaris probes, dissected samples were dehydrated in 70% EtOH overnight at 4°C. The probes were applied in the hybridisation buffer according to manufacturers' instruction, followed by a 4h incubation at 45°C. Subsequent washes were also performed at 45°C prior to mounting in Vectashield. For RNAscope a negative control probe was provided, targeted against the bacterial gene *dapB*.

For Burs stainings, flies were pre-starved for 22h prior to dissection and immunostaining to maximise retention of otherwise circulating Burs peptide in enteroendocrine cells[35].

Crop and intestinal transit measurements and assays

Crop size and fullness as well as transit of dye-laced food along the alimentary canal were assessed in response to certain diets, internal states and/or genetic manipulations. Virgin flies

of both sexes were collected and aged for either 4 or 7 days when raised at 25°C or 18°C respectively (tipped over to fresh food every 2 or 3 days respectively). Each group of flies was then either mated for 24h or kept as a virgin control group. After mating, flies were either starved overnight (14-16h) or kept feeding *ad libitum* on standard food. The next morning at 11am flies were gently transferred to tubes containing FCF Blue food by a single quick tap and allowed to feed *ad libitum* for 20min if previously starved, or 1-2h otherwise (see Temperature-controlled experiments). After feeding, flies were transferred by a single quick tap to a fresh empty fly-food vial and euthanised by snap freezing them in liquid nitrogen. Frozen tissues were either used for dissection directly or kept at -80°C (for analysis at a later stage). Tissues were never thawed and re-frozen. Experimental and control flies were all raised and assayed in the same batch of food for each experiment. For temperature-sensitive experiments we devised a simple home-made solution for temperature control that allows for real time monitoring of feeding behaviour. We named this the “sand incubator”. This comprised an empty metallic tray for fly vials filled with sand used for pet reptiles (Zoo Med WC-2 Repti-Sand, 4.5 Kg, Desert White) placed onto a heat mat (Exo Terra Heatwave Desert Heat Mat, 28 x 43 cm, Large). The mat’s temperature was controlled by a thermostat (HabiStat. Digital Temperature Thermostat + Timer). Fly vials were immersed in the sand for temperature control remaining available for undisturbed assaying of feeding behaviour. Tissues were dissected in 1.5x PBS (to avoid dye leaking out of the gut through small holes poked during dissection) and were either manually scored for crop size and food location, or transferred to a slide for brightfield imaging immediately after dissection.

Crop size and enlargement quantifications

Crop area and roundness measurements were conducted on segmented crops using the Fiji image analysis software[81]. For crop area, we used either the ‘Polygon’ or the ‘Wand’ tracing tools, using the ‘Default’ method in ‘Threshold Color’ to generate a binary mask that segmented blue-stained crops against a white background. Roundness corresponds to 4*area/(π*major_axis_2), or the inverse of the aspect ratio.

For crop shape analysis, 2 landmarks and 20 semi-landmarks were annotated for each crop using the ‘multipoint tool’ in the Fiji image analysis software[81]. Fixed landmarks were assigned to the base of the crop, where it meets the crop duct, and to a point diametrically opposed to this on the crop margin and along the axis of symmetry. 10 semi-landmarks were placed between each fixed landmark and allowed to slide between the immediate 2 neighbouring landmarks. Landmark coordinates were subjected to a Generalized Procrustes Analysis (GPA) to standardize for size, position and orientation, assuming bilateral symmetry. We analysed variation in crop shape using Principal Component Analysis (PCA) of the GPA aligned configurations of crop shapes and visualized these differences using thin plate spline (TPS) deformation grids. All morphometric analysis was performed using the ‘geomorph’ R package[82].

For a small subset of experiments (typically those that were confirmatory or negative), crop size was only assessed qualitatively; crop size was ranked as one of four categories: small (S), medium (M), large (L) and very large (VL).

In vivo crop enlargement assays

For live imaging of crop enlargement, virgin flies were collected and aged for 5 days at 25ºC and then either mated for 24h or kept as virgin. Flies were then starved for 2-3h before being briefly anaesthetised on ice (2-5mins) and mounted between two coverslips using a modified version of the Bellymount protocol[83] in which the flies were positioned over the edge of the coverslip to allow access to mouthparts for feeding. Mounting allowed crop and some loops of the midgut to be visible through the ventral surface of the abdomen. Flies were positioned with ventral side up and imaged on a Leica MZ165 FC attached to an S-View SXY-I30 camera. Flies were fed with liquid food containing Brilliant Blue FCF (2g Brilliant Blue FCF, 10g sucrose, 10g yeast extract, 200ml H_2O) using a narrow capillary for 3-5mins and then were imaged for a further 10mins. Time taken from first sip, to food visible in the crop, to food visible in the midgut was calculated.

Food intake and feeding behaviour assays

FlyPAD

FlyPAD assays were performed as described in ref. [37]. Half of the wells of a given flyPAD arena were filled with 2.4μL of food (5% yeast 7% dextrose in 1% agar), and the other half were either loaded with an agar control (1% agar) or left empty. For all experiments, flies were individually transferred to flyPAD arenas by mouth aspiration and allowed to feed for 1h at 25°C or 29°C and 65% relative humidity. The total number of sips per animal over this hour was acquired using the Bonsai framework[84], and analysed in MATLAB using previously described custom-written software[37]. Non-eating flies (defined as having fewer than two activity bouts during the assay) were excluded from the analysis. All flyPAD experiments were performed at the same time of the day between 11am and 1pm. Values shown in figures indicate the number of flies tested for each genotype. Data for experimental and control genotypes used for comparison were always acquired in the same flyPAD assay.

Blue dye-based assays

Quantification of ingested food was carried out using diets containing 1% FCF blue. Flies were allowed to feed (for up to 20min if pre-starved, and for up to 2h if previously fed *ad libitum*) and were then transferred by a single quick tap to a fresh empty fly food vial for snap freezing in liquid nitrogen. Frozen flies were transferred in groups of three to a clean 2mL PCR tube (Eppendorf, #22431048) with 0.5mL of water and a stainless-steel metal bead 5mm (QIAGEN, #69989). Fly tissues were homogenized using a QIAGEN TissueLyser II for 90sec at 30Hz. The samples were centrifuged at 10.000g for 5-10min. 0.2mL of the supernatant per fly was then directly transferred in to individual wells of a 96-well, flat bottom, optically clear plate (Thermo Fisher Sterilin, #611F96). A BMG Labtech FLUOstar Omega plate reader was used to measure dye content by reading the absorbance at 629nm. We used a standard curve of pure FCF blue dye to calculate the dye contented ingested per fly.

Fertility and fecundity assays

Virgin females were raised and aged for 7 days at 18°C, and then shifted to 29°C for the experiment. A group of 40 female flies of each of the three genotypes was used and crossed to 25 *OrR* males. The assays were performed in fly cages on apple juice plates with a smear of live yeast. The number of eggs laid per 24h window was manually counted using a hand-held counter device. To assess egg viability, 200 freshly laid eggs (laid over a 6h window) were collected for each genotype with a hook, split into 10 fresh food vials in groups of 20, and kept at 25°C until eclosion. The number of adults from each tube was scored.

Imaging

Brightfield imaging

Dissected crops and intestines were imaged using either a Leica MZ16F stereomicroscope attached to a DFC420 camera, or a Leica MZ165 FC attached to an S-View SXY-I30 camera.

Confocal imaging

A Leica SP5 confocal microscope was used to generate all confocal images. The images were acquired using both Leica HyD Photon counters as well as standard PMTs tailored for the fluorophores of each sample accordingly. For Flybow clones we used the built-in Leica channel unmixing algorithm post-imaging.

Quantifications of Ms neuron crop axonal terminals

The number of branches in crop terminals and their diameter were analysed using the NeuronStudio software[85].

In vivo calcium imaging

Ms-Gal4 flies were crossed to *UAS-GCaMP6f* (*attP40*) to drive the expression of the calcium reporter in Ms neurons. Virgin female flies from the progeny were collected and aged for 4-5 days. Flies were then either mated or kept virgin and used for imaging experiments. Flies were briefly anesthesized (5s) on ice and one fly was picked and glued for surgery. The proboscis was also glued to the thorax to limit motion artifacts during image acquisition. Surgery was performed to open the cuticle and obtain optical access to the brain as described previously[86]. During surgery and subsequent recordings, the aperture on the top of the fly head was bathed in an artificial haemolymph-like solution (130mM NaCl, 5mM KCl, 2mM $MgCl_2$, 2mM $CaCl_2$, 36mM sucrose, 5mM HEPES-NaOH; pH 7.3; 305mOsm).

Confocal imaging was performed under a scanning confocal microscope (Olympus BX61WI), using a water-immersion 20x objective (XLUMPlanFL, NA 1.0) and an excitation laser at 470 nm. The laser intensity was adjusted for each sample, but on average the laser power was similar between the two conditions (mated and virgin). Fluorescence recordings were performed at a rate of one image every 427ms in a single plane. To collect from the maximum number of cells, multiple planes were recorded consecutively in some samples.

Image analysis was performed offline with a graphical user interface, custom-programmed with MATLAB. Regions of interest (ROI) were delimited by hand and surrounding individual cell bodies of GCaMP6 expressing cells. Cells were classified as big or small based on expert knowledge of PI Ms neuronal anatomy (D.H.). After background subtraction, the absolute level of the 8-bit encoded fluorescence was calculated for each ROI as the mean over a time period selected for showing minimal fluctuations. Amplitude oscillation measurements were conducted as described in ref. [87].

Cell number quantifications, statistics and data presentation

For each experiment, a minimum of 10 samples per group were examined per genotype or condition. Experimental and control flies were bred in identical conditions, and were randomised whenever possible (for example, with regard to housing, position in tray). Control and experimental samples were dissected and processed at the same time and on the same slides, or assessed behaviourally simultaneously. All replicates were biological rather than technical and all measurements were taken from distinct samples. Experiments were typically repeated 3 times and only those experiments for which repeats gave comparable outcomes are included in the manuscript. Specific details of the number of experimental repeats for each experiment are provided in Supplementary Information. Experiments were controlled for sex, mating status, genotype and physiological state (for example starved or ad libitum-fed). Details are provided in Supplementary Information. No data points/outliers were excluded from our experiments and blinding was performed for a subset of experiments. Fly numbers are not limiting so no power calculations were used to pre-determine sample size. Oversampling was mitigated by choosing sample sizes based on previous knowledge of phenotypic variability in controls and other mutants, and by testing each hypothesis using at least two completely independent experimental approaches (e.g. use of mutation and *Gal4-UAS*-mediated RNAi downregulation).

Quantifications of fluorescence signal in brains of virgin and mated females and males stained for the anti-Ms antibody were performed using Fiji[81] measurements and the corrected total cell fluorescence (CTCF) metric. The brain samples used for these measurements were raised on the same food batch, dissected at the same time and stained on the same slide. They were then imaged applying the same imaging parameters.

For counts of Ms-positive, *CaLexA* activated cells, flies were dissected and stained 22h after mating along with virgin controls. These flies were raised on the same food batch, dissected at the same time and stained for Ms on the same slide. The same imaging parameters were applied to both groups and Ms- and GFP-positive cells were manually counted upon inspection of the entire brain.

Cell counts of enteroendocrine cells in the intestines of mated and virgin flies were performed 22-48h after mating. These samples were from flies raised on the same food batch, dissected at the same time and stained for Pros and Burs on the same slide. The same imaging parameters were applied. The posterior-most portion of the midgut was imaged using the Malpighian tubules at the level of the hindgut as a posterior-most landmark,

imaging the entire field of view within 20x or 63x magnification. The entire Z stack was used when manually counting cells using the Cell Counter plugin in Fiji[81].

All statistical analyses were carried out in GraphPad Prism 7.04. Statistical tests were typically two-sided. Comparisons between genotypes/conditions were analysed using Kruskal Wallis and Mann-Whitney-Wilcoxon tests for multiple or pairwise comparisons, respectively, conservatively assuming that data distributions were not parametric (as it is often the case for our data outputs). For egg laying experiments, a two-way ANOVA followed by a Tukey's multiple comparison test was used, considering day and genotype as independent factors. All graphs were generated using GraphPad Prism 7.04. Ranked crop values are displayed as percentages. All confocal and bright field images belonging to the same experiment and displayed together in our figures were acquired using the exact same settings. For visualisation purposes, level and channel adjustments were applied using ImageJ to the confocal images shown in the fig. panels (the same correction was applied to all images belonging to the same experiment), but all quantitative analyses were carried out on unadjusted raw images or maximum projections. In all experiments, n denotes the number of samples assayed and analysed for each genotype/condition (see Supplementary Information for full details). Data are presented as boxplots with all data points shown and the median (line) and min and max values (whiskers) plotted. Boxes encompass the 25th to 75th percentiles as calculated by GraphPad Prism 7.04. p-values are indicated as asterisks highlighting the significance of comparisons (non-significant (not shown): $p>0.05$; *: $0.05>p>0.01$; **: $0.01>p>0.001$; ***: $p<0.001$).

Europe PMC Funders Author Manuscripts

Extended Data

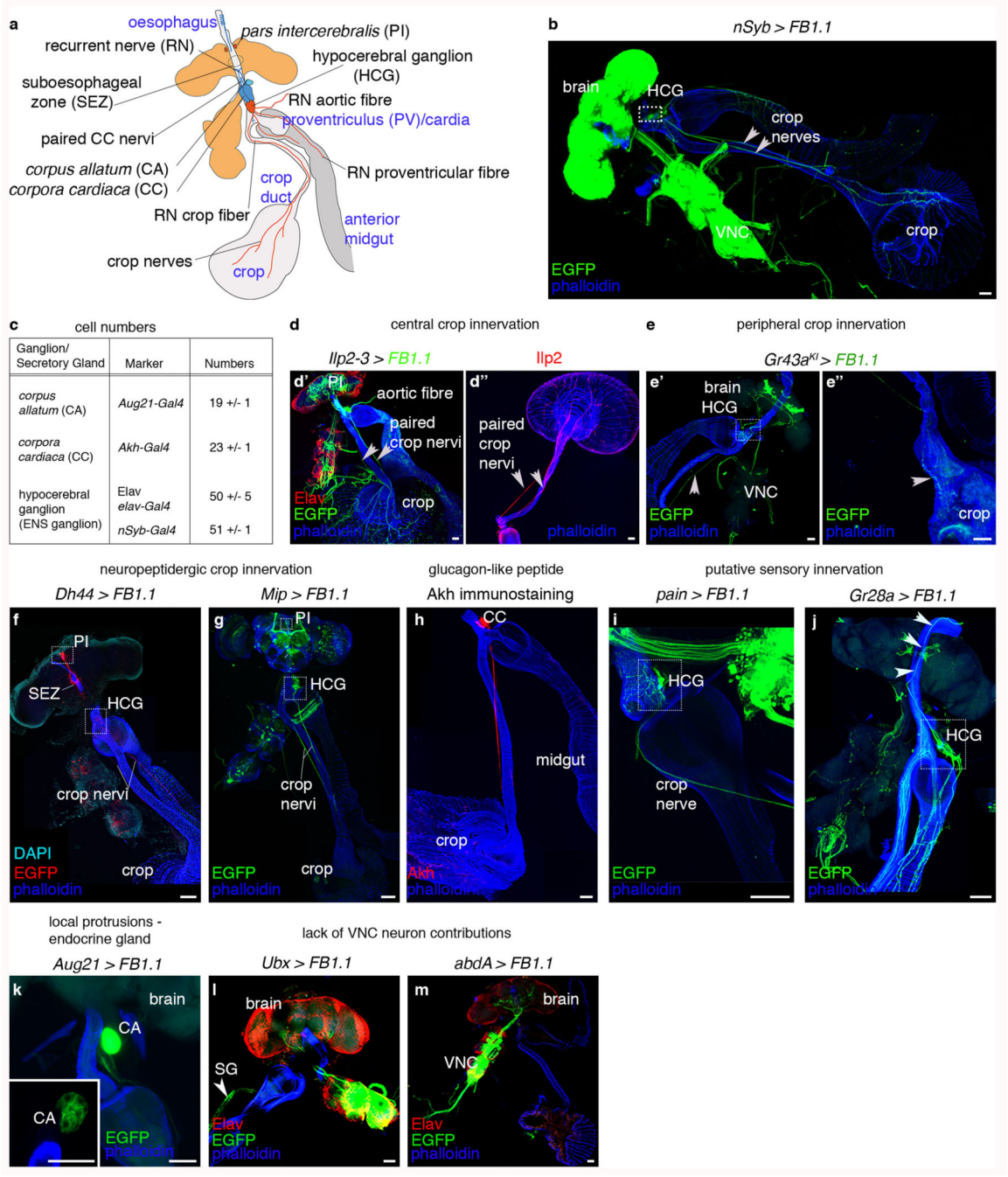

Extended Data Fig. 1. Innervation of the anterior portion of the adult *Drosophila* intestine

a, Schematic summary of the innervation of the anterior portion of the adult fly intestine, encompassing foregut, crop and anterior midgut. **b**, Pan-neuronal *nSyb-Gal4* driver expression visualised with EGFP (from *UAS-FB1.1* reporter) in green. Gut muscles are highlighted in blue with phalloidin staining. In all subsequent panels, driver expression is in green and phalloidin staining in blue. Abbreviations are as per **a**. **c**, Cell number

quantifications of the enteric nervous system (ENS) ganglia and secretory glands associated with the adult anterior midgut. **d-d″**, Direct innervation of the crop by neurons located in the central nervous system. **d'**, Projections emanating from the insulin-producing neurons in the PI (labelled with *Ilp2-3-Gal4*-driven expression of *UAS-FB1.1*-derived EGFP in green) innervate the crop and anterior midgut. Neuronal nuclei are labelled with anti-Elav antibody in red, and gut muscles are labelled in blue with phalloidin. **d″**, The axonal projections of these insulinergic neurons are visualised using immunostaining for Ilp2 peptide in red. **e-e″**, Innervation of the crop by peripheral neurons. Taste receptor-expressing neurons visualised with the *Gr43a*^{KI}*-Gal4* driver; gut muscles are labelled with phalloidin. The boxed area in **e'** highlights the cell bodies of ENS-like sensory neurons located in the HCG. **e″** shows the axonal terminals of the same sample on the crop muscle lobes (arrow). In **d-e″**, arrowheads point to the paired nerves innervating the crop. **f-j**, Spatially restricted *Gal4* drivers or antibodies reveal distinct crop-innervating neuronal subsets. In all panels, *Gal4* expression is visualised with EGFP (from *UAS-FB1.1* reporter) in green, and gut muscles are highlighted in blue with phalloidin staining. **f**, *Dh44-Gal4* expression. *Dh44-Gal4*-positive cell bodies in the PI (top dashed box) project to the HCG (bottom dashed boxed) and crop through the crop nervi. They also innervate the anterior midgut. No *Dh44-Gal4*-positive cell bodies are apparent in the HCG. DAPI labels the nuclei of the brain-gut axis in cyan. **g**, *Mip-Gal4*-positive cell bodies are found in both the PI and HCG (dashed boxes). Axons project to the anterior midgut, and along the crop nervi towards the crop. **h**, Glucagon-like adipokinetic hormone Akh (labelled with an anti-Akh antibody in red) is produced by cell bodies located in the paired *corpoca cardiaca* (CC) glands and is apparent in their projections along the crop nervi up to the junction between crop duct and lobes. **i**, Expression of a *pain-Gal4* reporter for *painless* (coding for a TRPA channel mediating detection of noxious heat and mechanical stimuli) in a subset of ENS neurons in the HCG (dashed box), pointing to possible mechanosensory identity. **j**, Expression of a *Gr28a-Gal4* reporter for *Gustatory receptor 28a* in two HCG cell bodies (dashed box), suggestive of chemosensory identity. Their neurites populate the anterior midgut and their axons project along the recurrent nerve (RN). **k**, The *Aug21-Gal4* reporter reveals short local projections from the *corpus allatum* around the foregut and anterior midgut. **l-m**, The use of Hox gene reporters allows labelling of large population of central neurons in thoracico-abdominal ganglion segments. No neurons in the *Ubx-Ga*l4 (**l**) or *abdA-Gal4* (**m**) expression domains contribute to the innervation of the crop of anterior midgut. *Gal4* expression is visualised with EGFP (from *UAS-FB1.1* reporter) in green, and gut muscles are highlighted in blue with phalloidin staining. Neuronal nuclei are visualised in red with anti-Elav (SG = salivary gland). Scale bars = 50μm. See Supplementary Information for a list of full genotypes, sample sizes and conditions.

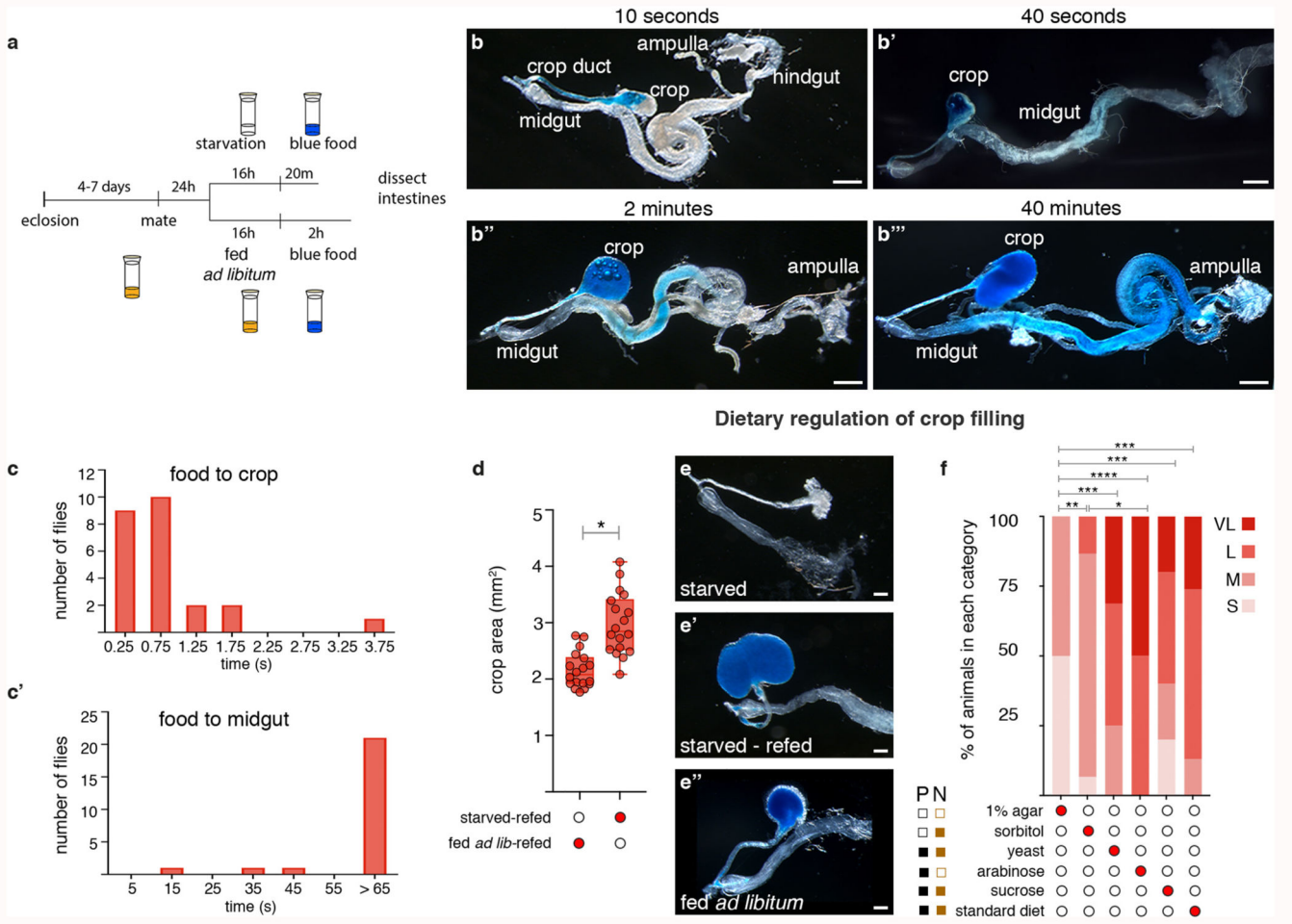

Extended Data Fig. 2. Intestinal transit dynamics and dietary regulation of crop enlargement

a, Cartoon summarising *ad libitum* and starvation/re-feeding assays using dye-laced food. **b-c'**, Transit of dye-laced food, intestinal transit at specific time points after ingestion. **b**, Gut dissected 10 seconds after feeding initiation; food is apparent in the crop duct and begins to enter the crop. **b'**, Gut dissected 40 seconds after feeding initiation; food fills the crop duct, crop, and begins to enter the midgut. **b″**, Gut dissected 2 minutes after feeding initiation; food fills the crop, crop duct and midgut. **b‴**, Gut dissected 40 minutes after feeding initiation; food fills the crop, crop duct, midgut and has now reached the hindgut and rectal ampulla. All panels show dissected adult fly intestines, anterior (left) posterior (right). **c,c'**, Frequency histogram derived from *in vivo* food ingestion videos (see Supplementary Video 1 for a representative example) showing higher number of flies with faster transit times of food to the crop (**c**) compared to midgut (**c**'). **d**, Quantification of crop area revealed that re-feeding after starvation results in larger crops than *ad libitum* feeding. **e-e″**, Representative dissected guts of a starved fly (**e**, 16h starvation on 1% agar), starved-refed fly (**e'**, 16h starvation on 1% agar, refed for 20min on dye-laced standard food), *ad libitum*-fed fly (**e″**, fed on dye-laced standard food for 2h). **f**, Ability of different food sources to elicit crop enlargement. These are categorized as palatable (P) and/or nutritious (N) using filled boxes if true and empty boxes if false (see Methods for further details of the different diets). In this

Europe PMC Funders Author Manuscripts

and all subsequent ranked data panels, crop size was ranked as one of four categories: small (S), medium (M), large (L) and very large (VL). Graphs are colour-coded from light to dark shades of red corresponding to increasing size of the crop. Data are displayed as percentages. Scale bars = 500μm. See Supplementary Information for a list of full genotypes, sample sizes and conditions. In all boxplots, line: median; box: 75th-25th percentiles; whiskers: minimum and maximum. All data points are shown. *: 0.05>p>0.01; **: 0.01>p>0.001; ***: p<0.001.

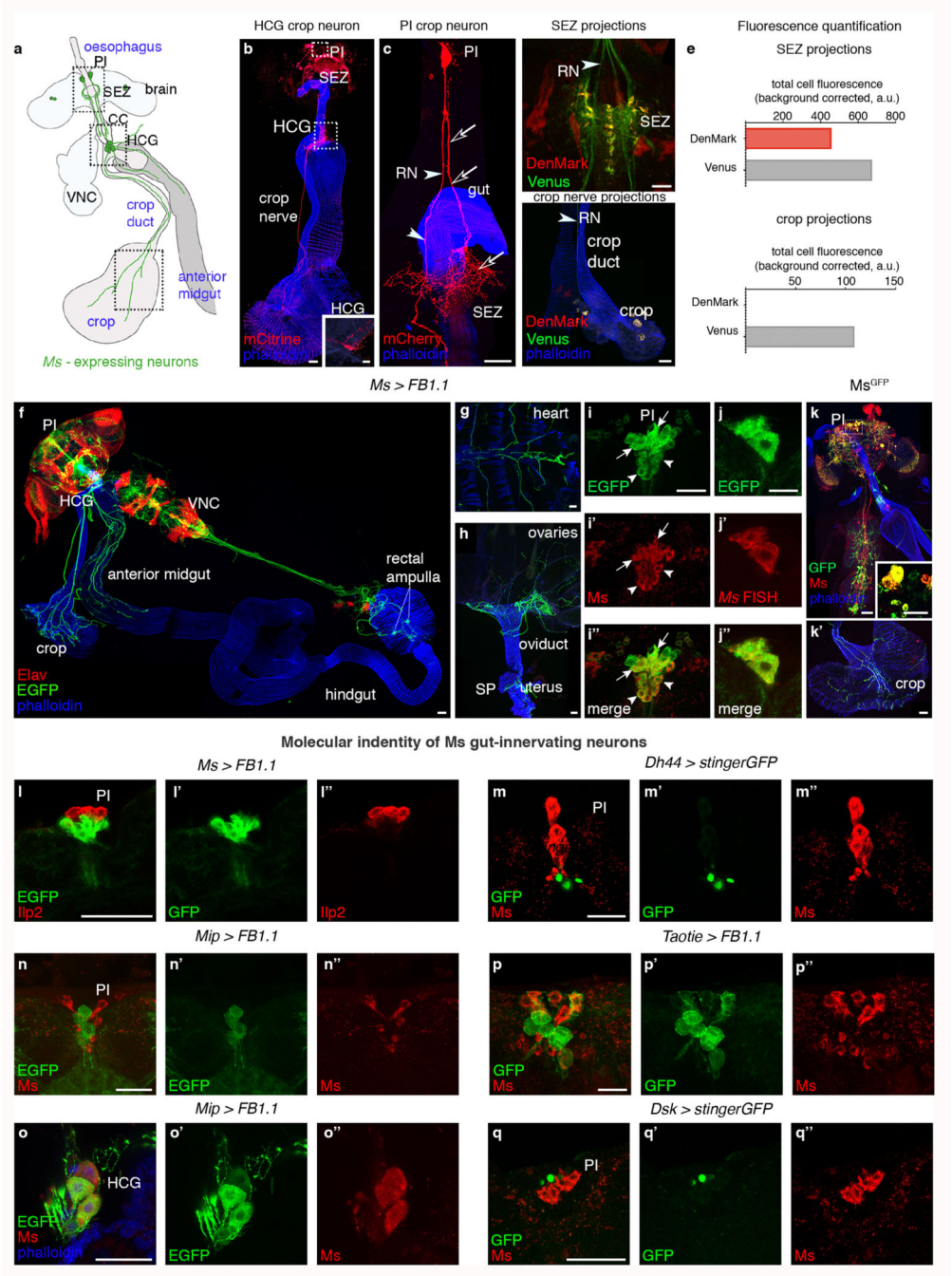

Europe PMC Funders Author Manuscripts

Extended Data Fig. 3. Characterisation of *Ms* expression

a, Cartoon depicting Ms neuronal subtypes. Dashed boxes highlight the main sites of Ms expression: ~ 30 neuronal cell bodies in the PI, ~ 5 enteric neurons located in the HCG and neuronal projections in the HCG and on the crop muscles. **b,c**, Single-cell Flybow clones of *Ms-Gal4*-expressing neurons (in red); gut muscle labelled with phalloidin (in blue). **b**, The PI and HCG where the Ms cell bodies reside are boxed. No Ms neurons have been labelled in the PI, but a single-cell, mCitrine-positive clone (in red) reveals an HCG neuron that innervates the crop muscle. Inset shows a single-cell clone of a second type of HCG *Ms-Gal4*-expressing neuron that only extends local projections. **c**, Single-cell FlyBow[44] clone of a large PI *Ms-Gal4*-expressing neuron. The main projection bifurcates, with one shorter (putatively dendritic) branch projecting towards the suboesophageal zone (SEZ) (empty arrows), and a longer (axonal) branch projecting towards the midgut/crop (arrows). **d,d'**, Co-expression of the dendritic marker DenMark (in red) and membrane marker Venus shown (in green) from *Ms-Gal4* reveals relative DenMark enrichment in their SEZ projections (**d**), consistent with dendritic nature. Venus enrichment is apparent in the crop nerve (**d'**), consistent with its axonal identity. Top left arrow points to the crop nerve, and bottom arrow points to where it terminates. **e,** Quantification of fluorescence for DenMark and Venus in SEZ (top) crop nerve (bottom) projections. **f-j″**, *Ms-Gal4* expression, visualized by EGFP from the *UAS-FB1.1* reporter (in green). **f**, Overview of *Ms-Gal4*-positive intestinal innervation; *Ms*-positive neurites are apparent on the crop, anterior midgut and posterior hindgut (rectal ampulla). Neuronal nuclei are stained with an anti-Elav antibody in red, and gut muscles are labelled in blue with phalloidin. **g**, *Ms-Gal4* expression in heart-innervating neurons; heart muscles are labelled in blue with phalloidin. **h**, *Ms-Gal4* expression in peripheral neurons that innervate the ovaries, oviduct and spermatheca (SP). **i-i″,** Co-expression of *Ms-Gal4* and Ms peptide (in red) in a cluster of PI neurons; arrows and arrowheads point to big and small PI Ms neuron subtypes, respectively. **i** and **i'** show single channel images for *Ms-Gal4* and anti-Ms antibody, respectively. The merged image is shown in **i″**. **j-j″**, Co-expression of *Ms-Gal4* and *Ms* transcript (visualised using single-molecule RNA fluorescence *in situ* hybridisation in red) in the same cluster of PI neurons. **j** and **j'** show single channel images for *Ms-Gal4* and *Ms* transcript, respectively. The merged image is shown in **j″**. **k-k'**, Ms protein reporter expression (in green). Ms peptide is in red and gut muscles are labelled with phalloidin in blue. **k**, Co-expression between the Ms protein reporter Ms peptide in the nervous system, and in neuronal projections towards the gut. Ms and the Ms protein reporter are co-expressed by the PI Ms neurons (boxed and inset). **k'**, The Ms protein reporter also labels axonal projections innervating the crop muscles. **l-q″**, Expression (or lack thereof) of neuropeptides and other markers in the Ms-expressing neurons in the PI or HCG. For each letter, the first panel shows double staining, the second and third panels show single channels for clarity, **l-l″**, PI Ms neurons do not co-express Ilp2, used as a marker of insulin-producing neurons. **m-m″**, PI Ms neurons do not co-express *Dh44-Gal4*, used as a marker of Diuretic Hormone 44-producing neurons. **n-n″**, PI Ms neurons do not co-express *Mip-Gal4*, used as a marker of Myoinhibiting peptide precursor-producing neurons. **o-o″**, Co-expression between Ms and *Mip-Gal4* in 3 out of the 5 HCG Ms-expressing neurons. Phalloidin was used to label gut muscles (in blue). **p-p''**, A subset of PI Ms neurons co-express *Taotie-Gal4*; other *Taotie-Gal4*-positive PI neurons are Ms-negative. In the HCG, *Taotie-Gal4* expression is only apparent inconsistently in one Ms

neuron (data not shown). **q-q″**, PI Ms neurons do not co-express *Dsk-Gal4*, used as a marker of Drosulfakinin-producing neurons. Scale bars: **b, d', f-h** and **k-k'** = 50μm, **i-j″, l-o ″** and **q-q″** = 25μm, **b** (inset), **c**, **d, p-p″** = 20μm and **k** (inset) = 10μm. See Supplementary Information for a list of full genotypes, sample sizes and conditions.

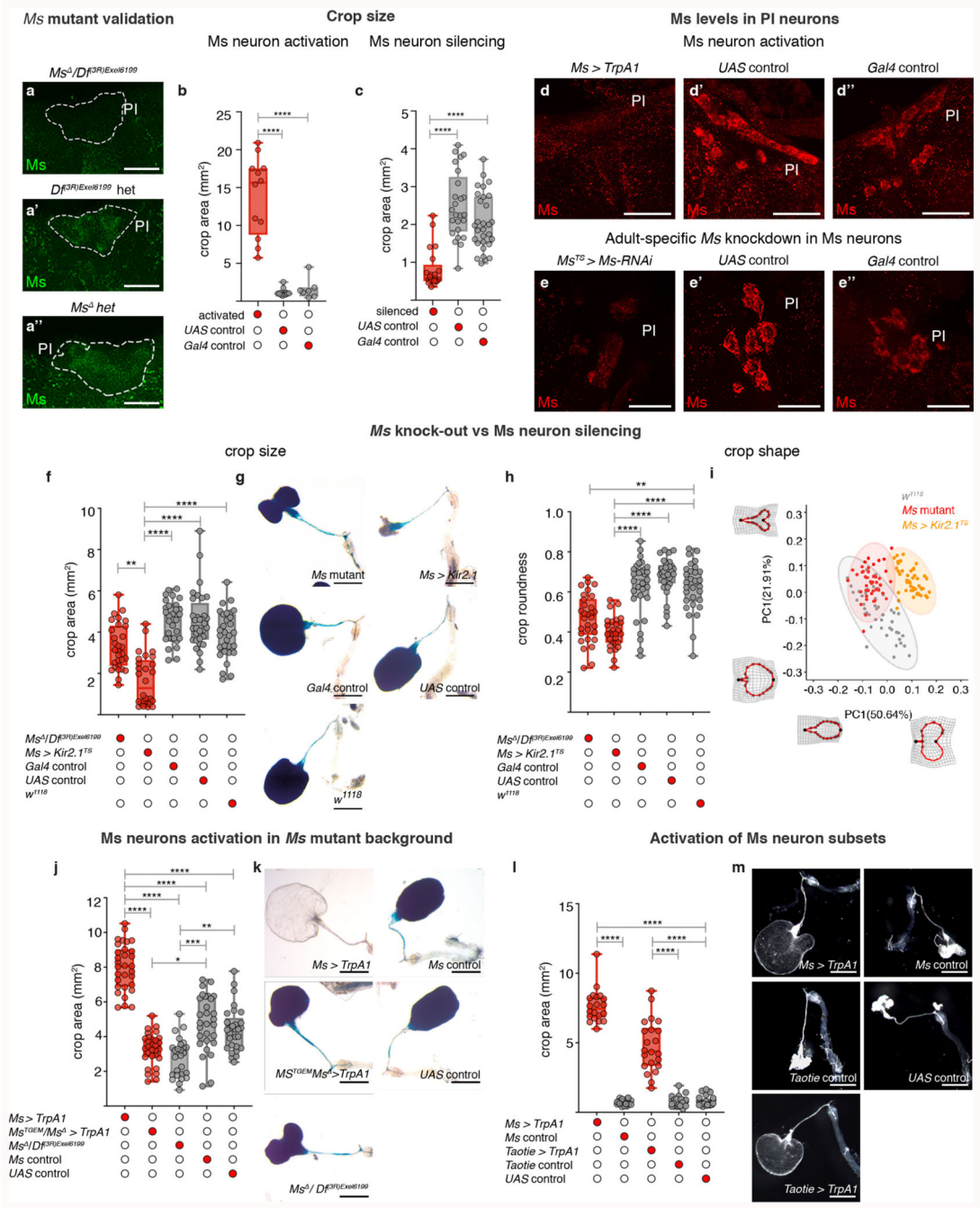

Extended Data Fig. 4. Ms neuron regulation of crop enlargement

a-a', Validation of Ms^{Δ} mutant using anti-Ms staining shown in green; PI is highlighted by dashed lines. **a**, Lack of Ms staining in the PI of *Ms* mutants (Ms^{Δ}/ *Df(3R)Exel6199*). Ms

Europe PMC Funders Author Manuscripts

staining is apparent in the PI of *Df(3R)Exel6199* (**a'**) and Ms^{Δ} (**a″**) heterozygous control flies. **b,** Quantifications of crop area in *ad libitum*-fed flies upon *Ms-Gal4*-driven TrpA1 expression (4h at the permissive temperature), showing these have significantly larger crops relative to *UAS* and *Gal4* controls. **c**, Quantifications of crop area in starved-refed flies upon *Ms-Gal4*-driven *Kir2.1* expression (temporally confined with $tub\text{-}Gal80^{TS}$), showing these have significantly smaller crops relative to *UAS* and *Gal4* controls. **d-e″**, Effect of neuronal activation and *Ms* downregulation on Ms levels in PI neurons. Thermogenic activation of Ms neurons in *ad libitum* fed flies depletes Ms peptide (in red) from Ms neuron cell bodies in the PI (**d**) compared to *UAS* (**d'**) and *Gal4* (**d″**) controls. Adult-specific *Ms* downregulation in Ms neurons of starved-refed flies results in reduced Ms staining (red) in PI neurons (**e**), compared to *UAS* (**e'**) and *Gal4* (**e″**) controls. **f-i**, Effect of *Ms* loss-of-function and adult-specific Ms neuron inactivation on crop expansion and shape, upon starvation-refeeding in mated females. **f,** Quantifications of crop area revealed that Ms neuron inactivation results in smaller crops relative to *Ms* mutant or w^{1118}, *UAS* and *Gal4* controls. **g,** Representative crop images of genoytpes quantified in **f**. **h**, Quantifications of crop roundness revealed that crops are less round upon Ms neuron inactivation or in *Ms* mutant compared to w^{1118}, *UAS* and *Gal4* controls. **i**, PCA of landmark position variation along the crop outline, showing that crop shapes are distinct between *Ms* mutant (red), Ms neuron inactivation (yellow) and w^{1118} (grey), being more similar between *Ms* mutant and w^{1118}, as highlighted by partial overlap of their 95% confidence ellipses. Wireframe deformation grids are shown to illustrate the mininum and maximum shape deviations as compared to the mean shape along each PC axis. **j-k**, Effect of Ms neuron activation on crop expansion in *Ms* mutant background, upon starvation-refeeding in mated females. **j**, Quantifications of crop area show that activation of Ms neurons by *Ms-Gal4*-driven *TrpA1* expression resulted in larger crops relative to activation of Ms neurons by Ms^{TGEM}-driven *TrpA1* expression in an heteroallelic mutant background, as well as relative to *Ms* mutant or *UAS* and *Gal4* controls. **k**, Representative crop images of genoytpes quantified in **j**. **l-m**, Effect of Ms and *Taotie* neuron activation on crop enlargement, upon starvation in mated females. **l**, Quantification of crop area shows that activation of either Ms neurons or *Taotie* neurons resulted in larger crops compared to respective *Gal4* controls and *UAS* control, even in the absence of food. **m**, Representative crop images of genotypes quantified in **l**. Scale bars: **a-a'** = 10μm, **d-e″** = 25μm, **g, k** and **m** = 500μm. See Supplementary Information for a list of full genotypes, sample sizes and conditions. In all boxplots, line: median; box: 75^{th}-25th percentiles; whiskers: minimum and maximum. All data points are shown. *: 0.05>p>0.01; **: 0.01>p>0.001; ***: p<0.001.

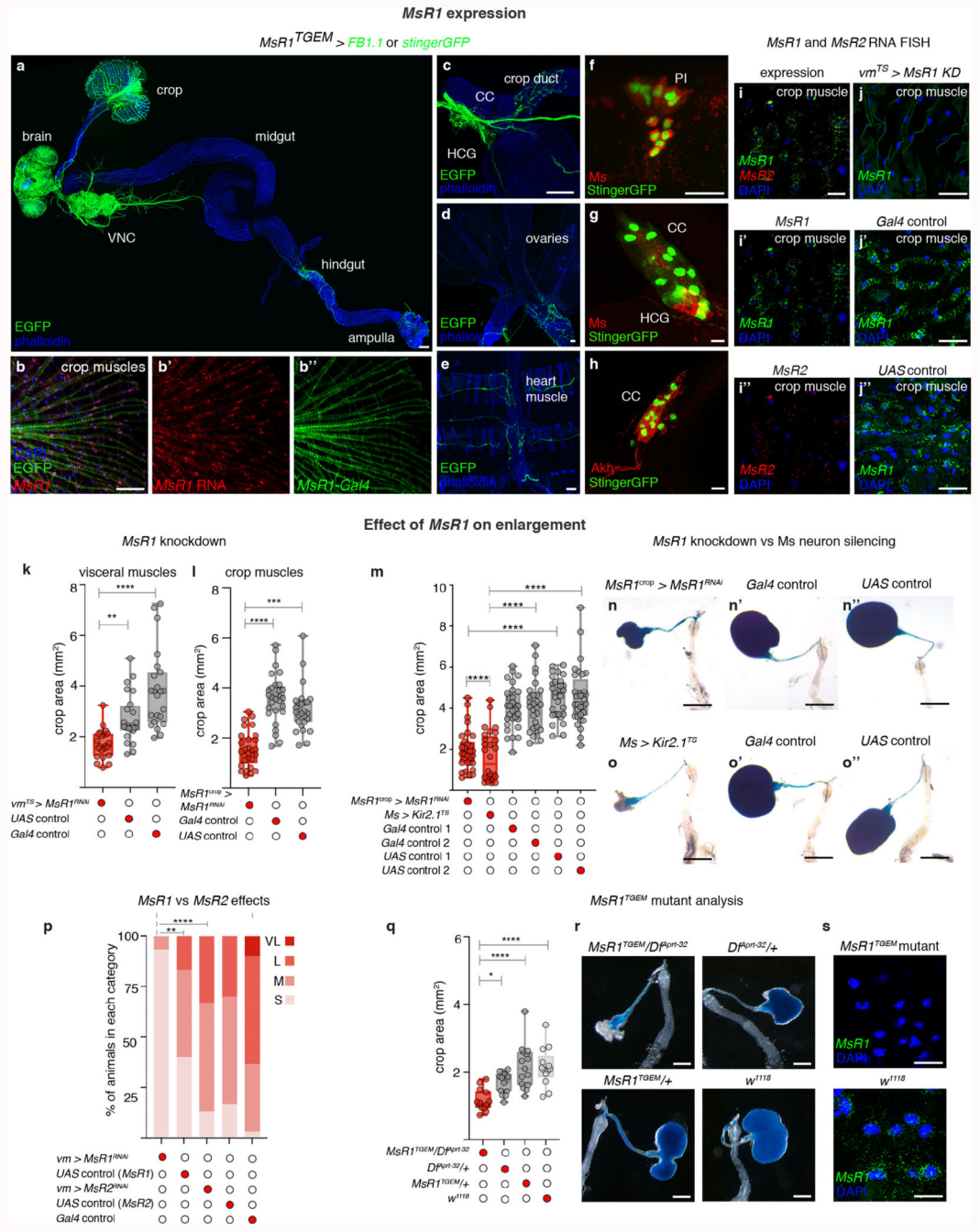

Extended Data Fig. 5. Expression of Ms receptors and their regulation of crop enlargement

a, FB1.1-derived EGFP reveals *MsR1* expression in the crop muscles and nervous system, including nerves innervating the crop, hindgut and rectal ampulla. In this and subsequent panels, muscles are labelled with phalloidin (in blue). **b-b″**, Co-expression between *MsR1* mRNA stained with single-molecule RNA fluorescence *in situ* hybridisation (**b,b'**, in red) and FB1.1-derived EGFP driven by *MsR1*^{TGEM}*-Gal4* (**b**,**b″,** in green) is observed in crop muscles. Muscle nuclei are shown in blue with DAPI; single channels are shown for clarity. **c**, Detail of the HCG and *corpora cardiaca* (CC); the latter is extensively innervated by

Europe PMC Funders Author Manuscripts

MsR1-expressing neurons. **d**, FB1.1-derived EGFP reveals *MsR1* expression in neurons innervating the female reproductive system, but not in its muscles. **e**, FB1.1-derived EGFP reveals *MsR1* expression in heart-innervating neurons, but not in heart muscles. **f,** Higher magnification image of the central brain; nuclear GFP reveals broad *MsR1* expression in neurons including the PI Ms neurons shown with Ms staining (in red). **g**, A subset of 2-3 MsR1-positive neurons in the HCG co-express Ms. **h,** Nuclear GFP reveals *MsR1* expression overlaps with Akh staining in CC cells (in red). **i**, Single-molecule fluorescence *in situ* hybridisation of *MsR1* and *MsR2* mRNAs in crop muscles; *MsR1* (in green) is more readily detected than *MsR2* (in red). Muscle cell nuclei are shown in blue by DAPI staining. The MsR1 expression described in **a-h** is consistent with transcriptomics data[88,89]. **i'** and **i″** show single MsR1 or MsR2 channels for clarity. **j-j'**, Validation of adult-specific *MsR1* knockdown in visceral muscles (vm^{TS} > *MsR1-RNAi*). Panels show high magnification images of crop muscles. *MsR1* mRNA expression is visualised by single-molecule RNA fluorescence *in situ* hybridisation (in green) in $vm\text{-}Gal4^{TS}$ (**j**), but it is reduced/absent from *MsR1* knockdown crops (**j'**). **k**, Quantifications of crop area in starved-refed flies upon downregulation of *MsR1* in visceral muscles, showing that crop size is visibly reduced upon *MsR1* downregulation compared to *UAS* and *Gal4* controls. **l**, A similar reduction in crop area is also quantified upon *MsR1* downregulation specifically in crop muscles using a different driver line ($MsR1^{crop}$ > $MsR1^{RNAi}$). $MsR1^{crop}$-*Gal4* is *MsR1-Gal4, nsyb-Gal80*, in which *MsR1-Gal4* neuronal expression is prevented using the pan-neuronal *nsyb-Gal80* driver, rendering it a crop muscle-specific driver. **m-o″**, Effect of crop muscle-specific downregulation of *MsR1* on crop size. **m,** Quantifications of crop area in starved-refed mated females shows that crop-specific downregulation of *MsR1* ($MsR1^{crop}$ > $MsR1^{RNAi}$) resulted in reduced crop areas, similar to Ms neuron inactivation (*Ms* > *Kir2.1*) and significantly reduced as compared to *Gal4* and *UAS* controls. **n-o″**, Representative crop phenotypes of the genotypes quantified in **m**. **p**, Quantification of crop area upon visceral muscle-specific *MsR1* and *MsR2* downregulation, showing that *MsR1* knockdown, but not *MsR2* knockdown, resulted in reduced crop sizes, as compared to *UAS* and *Gal4* respective controls. **q**, Quantifications of crop area in starved-refed mated females shows that heteroallelic $MsR1^{TGEM}/Df^{Aprt\text{-}32}$ mutants have reduced crop areas relative to w^{1118} or heterozygous controls. **r**, Representative crop images from genotypes quantified in **q. s**, Validation of *MsR1* mutation and *MsR1* fluorescence *in situ* hybridisation signal specificity. *MsR1* mRNA (green) is absent from the crop muscle cells of $MsR1^{TGEM}$ mutants, and apparent in w^{1118} control flies. Scale bars: **b-b″**, **f-j″** and **s** = 10μm, **a, c, d, e** = 50μm, **r** = 500μm and **n-o″** = 1mm. See Supplementary Information for a list of full genotypes, sample sizes and conditions. In all boxplots, line: median; box: 75th-25th percentiles; whiskers: minimum and maximum. All data points are shown. *: 0.05>p>0.01; **: 0.01>p>0.001; ***: p<0.001.

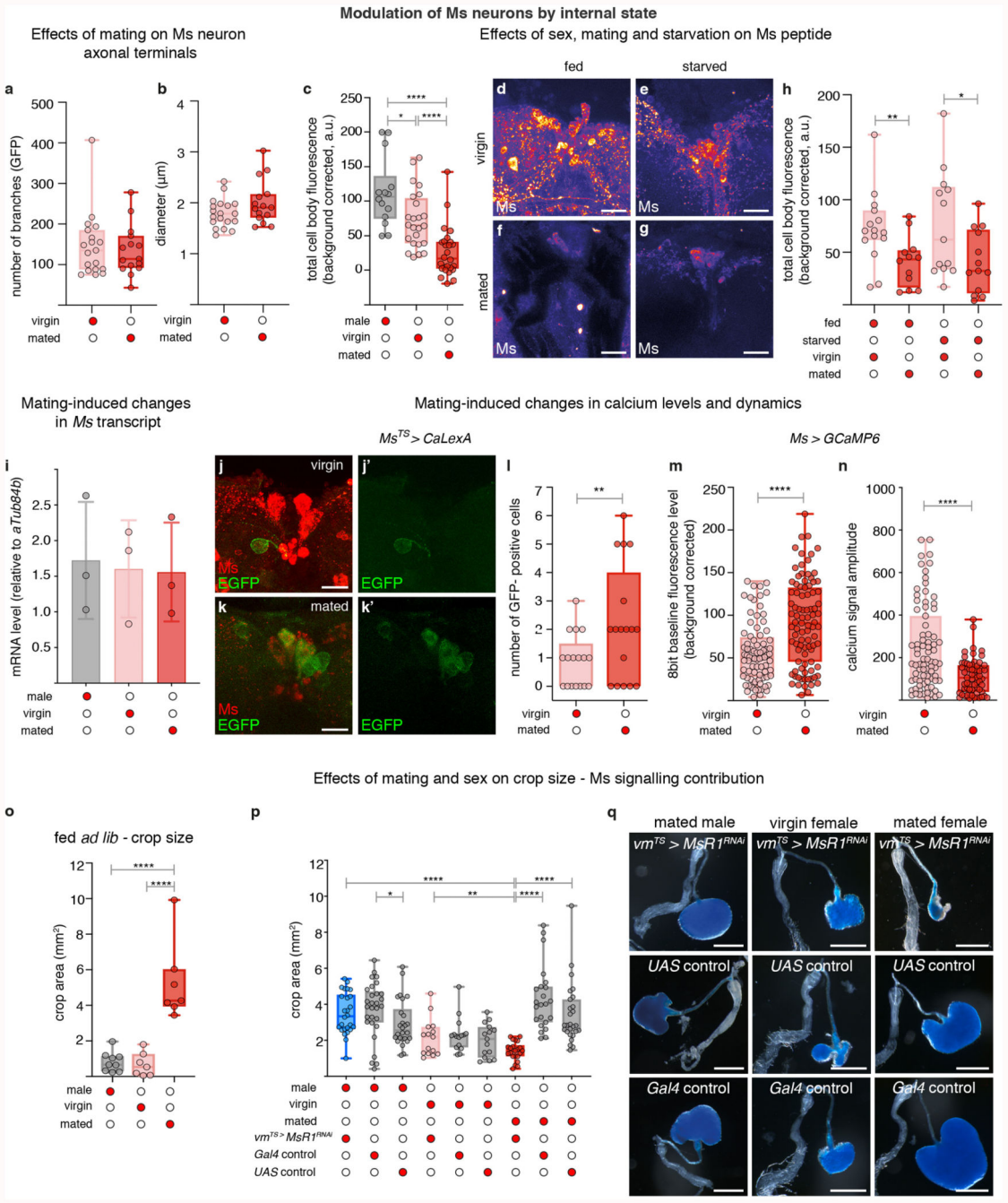

Extended Data Fig. 6. Post-mating modulation of Ms neurons

a-b, Analysis of Ms neuron crop terminals in virgin and mated females. Neither the number of axonal branches (**a**) nor their diameter (**b**) is significantly different between virgin and mated females. **c**, Quantifications of Ms staining levels in the cell bodies of PI neurons of wild-type, *ad libitum*-fed males, virgin females and mated females. Mated females have less Ms peptide than virgin females or males; virgin females have less peptide than males. **d-h,** Comparison of Ms peptide levels in the cell bodies of PI neurons in fed versus starved virgin and mated females. Representative images of Ms staining in the cell bodies of the PI neurons

Europe PMC Funders Author Manuscripts

Europe PMC Funders Author Manuscripts

of fed virgin females (**d**), starved virgin females (**e**), fed mated females (**f**) and starved mated females (**g**). **h**, Quantification of Ms staining in the cell bodies of PI neurons shows that Ms levels are reduced in mated females compared to virgins, irrespective of fed or starved status. **i**, RT-qPCR expression data for *Ms* transcript levels in the brain of *ad libitum*-fed, control males (grey column), virgin females (pink column) and mated females (red column). No significant differences are apparent between groups. **j-l**, CaLexA-based assessment of mating-triggered changes in PI Ms neuronal activity, achieved by adult- and Ms-confined CaLexA expression ($Ms^{TS} > CaLexA$). Representative images of *ad libitu*m-fed, wild-type virgin (**j,j'**), and mated females (**k,k'**) are shown. Ms neurons are labelled with anti-Ms antibody (in red) and CaLexA channel is shown as a single channel (in green), for clarity. **l**, Quantification of *CaLexA*-derived GFP-positive cells in PI Ms neurons of virgin (pink box) and mated (red box) females, showed that fewer cells are CaLexA-positive in virgin compared to mated females; each data point corresponds to a different brain. **m,n**, Quantification of baseline GCaMP fluorescence (corrected for background) (**m**) and amplitude of GCaMP fluorescence oscillations (**n**) in the cell bodies of PI Ms neurons of virgin females (pink box) or mated females (red box). Each data point corresponds to an individual cell measurement. Higher GCaMP signal and reduced oscillation amplitude are detected in mated females. **o**, Crop area quantifications in wild-type, *ad libitum*-fed males, virgin females and mated females. The crop of mated females is bigger than that of virgin females or males. **p,q,** Effects of sex and mating status on Ms signalling contribution to crop size. **p**, Quantification of crop area upon adult-specific downregulation of *MsR1* in visceral muscles shows that this was significantly reduced in mated females but not in males or virgin females, as compared to respective controls. **q**, Representative crop images of genotypes quantified in **m**. Scale bars: **d-g** and **j-k'**= 20μm and **q** = 500μm. See Supplementary Information for a list of full genotypes, sample sizes and conditions. In all boxplots, line: median; box: 75th-25th percentiles; whiskers: minimum and maximum. All data points are shown. *: 0.05>p>0.01; **: 0.01>p>0.001; ***: p<0.001.

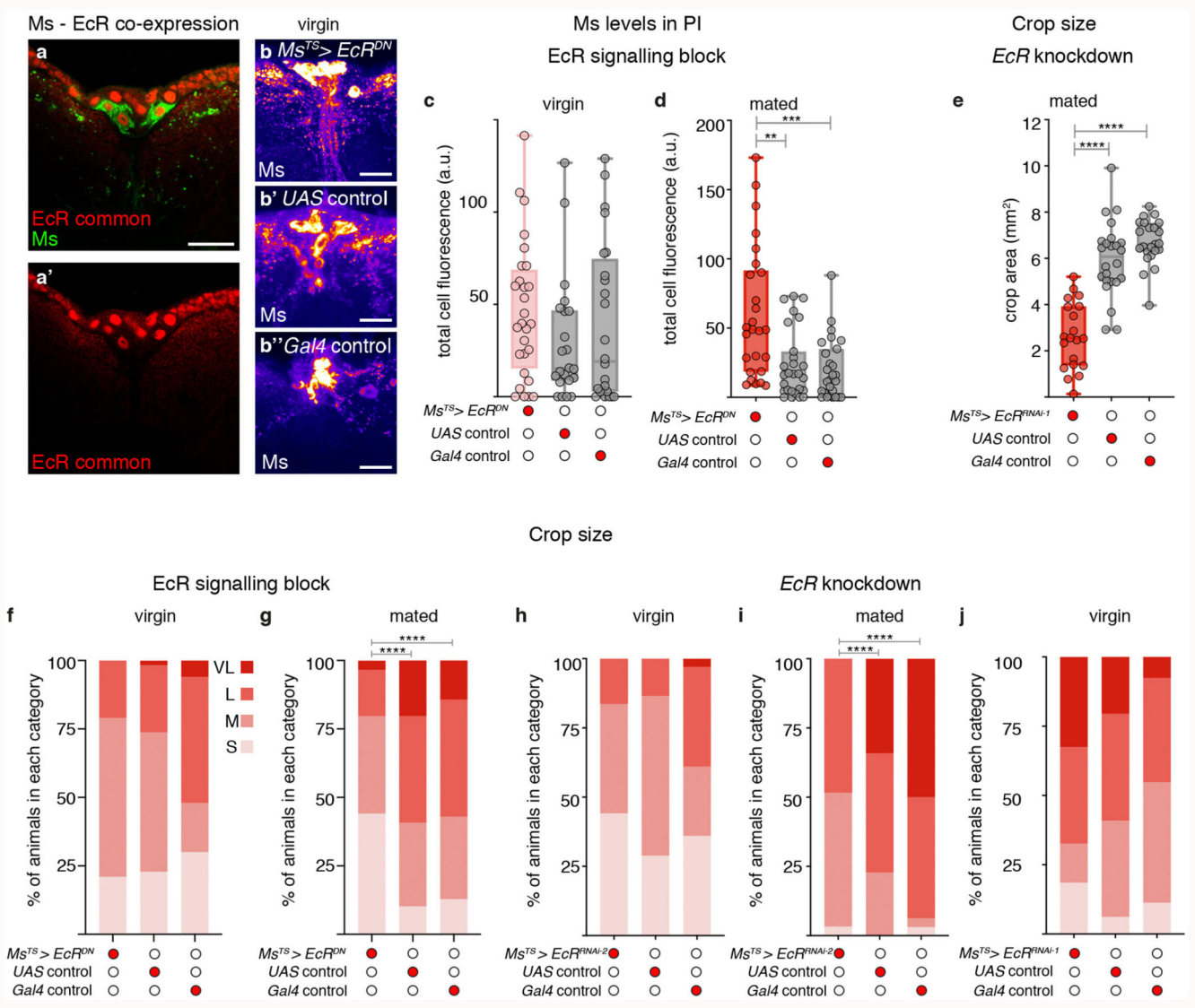

Extended Data Fig. 7. Ecdysone modulation of Ms neurons and crop size

a-a', Expression of EcR in PI Ms neurons. Ms staining (in green) (**a**) and EcR staining (in red) (**a'**) overlap and are shown as single channels for clarity. **b-d,** Ecdysone effect on Ms levels in PI neurons. Representative images show comparable Ms levels upon expression of *EcR*^{DN} in virgin females (**b**) relative to *UAS* (**b'**) and *Gal4* (**b″**) controls. Fluorescence signals are pseudo-coloured; high to low intensity is displayed as warm (yellow) to cold (blue) colours. **c**, Quantification of Ms staining intensities in PI neurons of virgin females upon expression of *EcR*^{DN} showed comparable levels to *UAS* and *Gal4* controls. **d**, Quantification of Ms staining intensities in PI neurons of mated females upon expression of *EcR*^{DN} showed increased Ms levels relative to *UAS* and *Gal4* controls. **e**, Quantification of crop area in starved-refed mated females revealed smaller crops upon adult- and Ms neuron-specific *EcR* downregulation compared to *UAS* and *Gal4* controls. **f-j**, Classification of crop size upon expression of EcR^{DN} (**f-g**) or *EcR* downregulation (**h-j**) in starved-refed female flies. Distribution of crop sizes did not significantly change relative to *UAS* and *Gal4*

Europe PMC Funders Author Manuscripts

controls in virgin females (**f, h, j)**. In mated females, the distribution shifted towards smaller crop sizes, relative to *UAS* and *Gal4* controls (**g, i**). Ranked data are displayed as percentages. Scale bars = 20μm. See Supplementary Information for a list of full genotypes, sample sizes and conditions. In all boxplots, line: median; box: 75th-25th percentiles; whiskers: minimum and maximum. All data points are shown. *: 0.05>p>0.01; **: 0.01>p>0.001; ***: p<0.001.

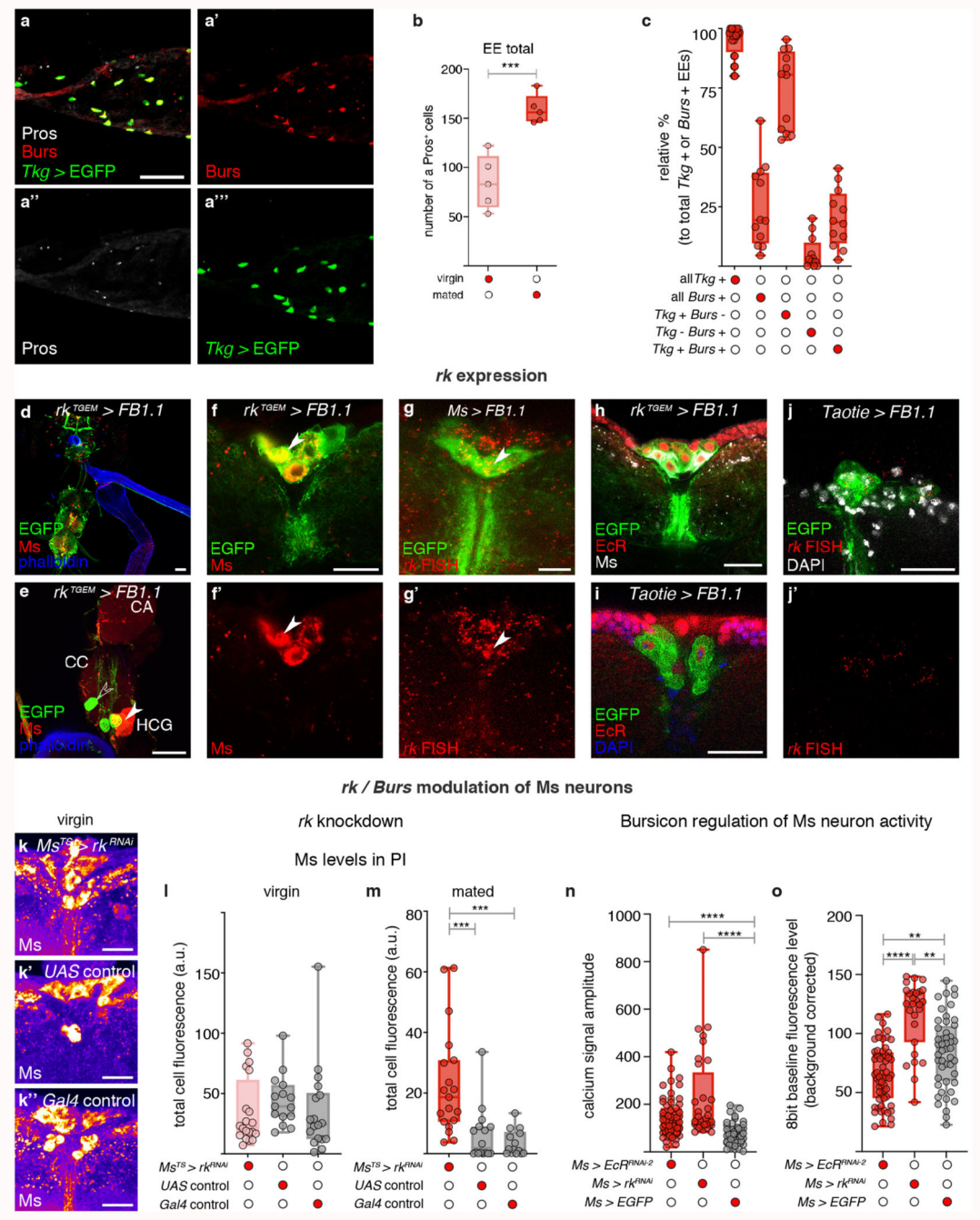

Extended Data Fig. 8. Bursicon modulation of Ms neurons

Europe PMC Funders Author Manuscripts

a, Co-expression of Burs (**a'**, in red), Pros (**a″**, in white) and GFP driven by *Tkg-Gal4* (**a‴**, in green) in midgut enteroendocrine cells of mated females. **b**, Quantifications of Pros-positive midgut cells shows increased enteroendocrine cell number in mated females relative to virgins. Flies were starved for 22h to increase Burs staining in the enteroendocrine cell bodies[35]. Single channels for each marker are shown for clarity. **c**, Quantification of enteroendocrine cells of mated females labelled by *Tkg-Gal4*-driven EGFP and Burs staining (such as that shown in **a**). More *Tkg-Gal4*-positive than Burs-positive enteroendocrine cells are apparent. The majority of Burs-positive enteroendocrine cells are *Tkg-Gal4*-positive. **d-e**, Co-expression of rk^{TGEM} (driving *FB1.1*, in green) with Ms peptide (in red) is shown in brain and VNC neurons (**d**), and in the HCG ganglion (**e**). **f-f',** Co-expression of rk^{TGEM} (driving FB1.1-derived EGFP, in green) with Ms peptide (in red) was observed brain PI neurons. **f'**, Ms staining is shown as a single channel for clarity. **g-g'**, Co-expression of *Ms-Gal4* (driving FB1.1-derived EGFP, in green) with *rk* mRNA (stained with fluorescence *in situ* hybridisation, in red) was observed in brain PI neurons. **g'**, *rk* fluorescence *in situ* hybridisation signal is shown as a single channel for clarity. **h**, Co-expression of rk^{TGEM} (driving FB1.1-derived EGFP, in green) with Ms peptide (in white) and EcR (in red) was observed in brain PI neurons. **i**, Co-expression of *Taotie-Gal4* (driving FB1.1-derived EGFP, in green) with EcR (in red) was observed in brain PI neurons. Nuclei are stained with DAPI (in blue). **j-j'**, Co-expression of *Taotie-Gal4* (driving FB1.1-derived EGFP, in green) with *rk* mRNA (stained with fluorescence *in situ* hybridisation, in red) was observed in brain PI neurons. Nuclei are stained with DAPI (in white). **j'**, *rk* mRNA fluorescence *in situ* hybridisation signal is shown as a single channel for clarity. **k-m**, *rk* regulation of Ms levels in PI neurons. Representative images show similar Ms staining signal upon adult-specific *rk* downregulation in virgin females (**k**) relative to *UAS* (**k'**) and *Gal4* (**k″**) controls. Fluorescence signals are pseudo-coloured; high to low intensity is displayed as warm (yellow) to cold (blue) colours. **l**, Quantification of Ms staining intensities in PI neurons of virgin females upon adult-specific *rk* downregulation showed comparable levels to *UAS* and *Gal4* controls. **m**, Quantification of Ms staining intensities in PI neurons of mated females upon adult-specific *rk* downregulation showed increased Ms levels relative to *UAS* and *Gal4* controls. **n**, Quantification of the amplitude of GCaMP oscillations in PI neurons of mated females shows that downregulation of *EcR* and *rk* in Ms neurons significantly increased the amplitude of calcium signal. **o,** Quantification of GCaMP baseline fluorescence levels in PI neurons of mated females revealed that downregulation of *EcR* in Ms neurons significantly reduced GCaMP signal, whereas downregulation of *rk* increased GCaMP signal, both relative to expression of EGFP. Hence, calcium oscillations become virgin-like both upon *EcR* or *rk* downregulation, whereas their effects on overall calcium fluorescence are different. Scale bars = 20μm apart from **a-a″** and **d-e** = 50μm. See Supplementary Information for a list of full genotypes, sample sizes and conditions. In all boxplots, line: median; box: 75th-25th percentiles; whiskers: minimum and maximum. All data points are shown. *: 0.05>p>0.01; **: 0.01>p>0.001; ***: p<0.001.

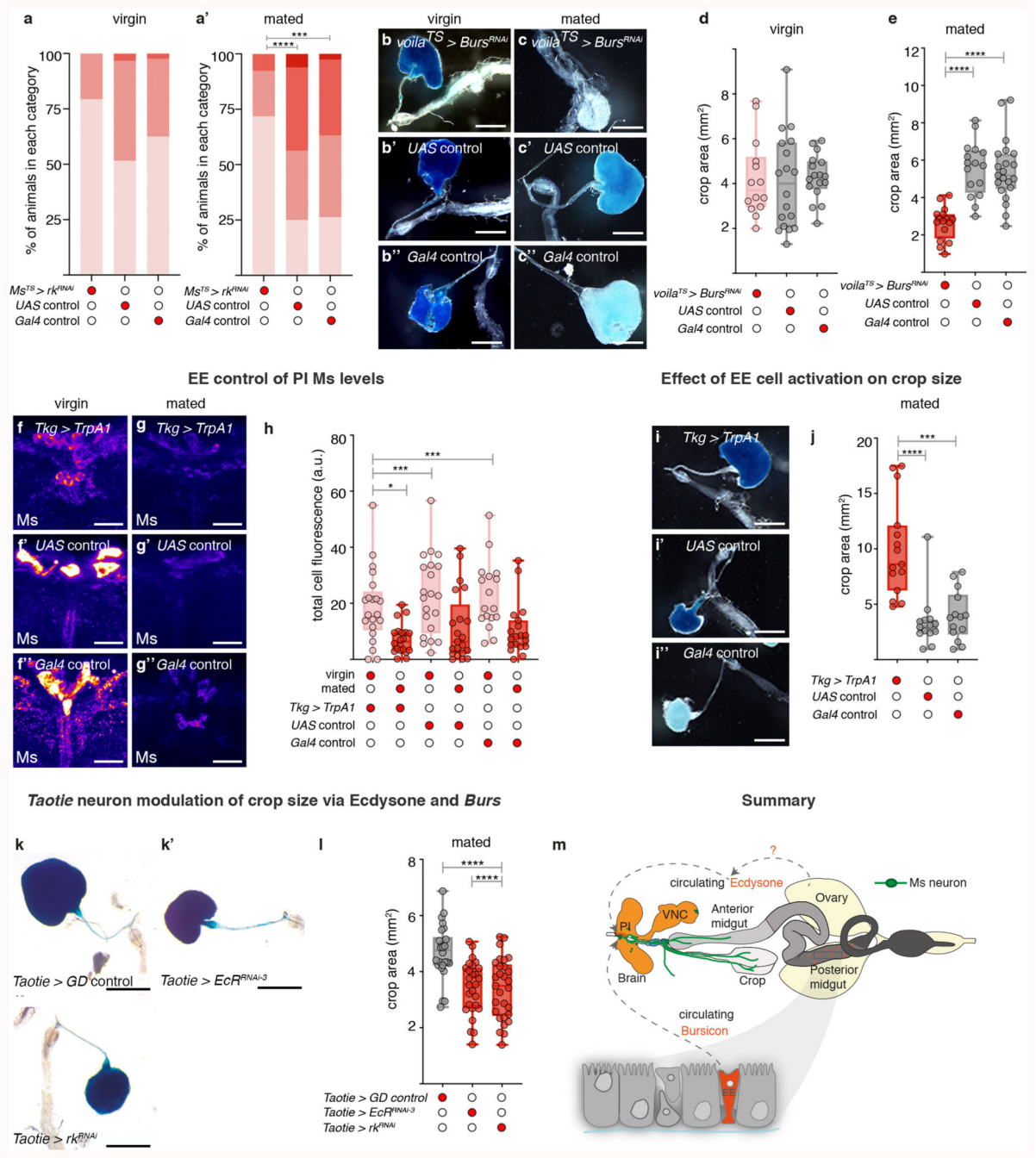

Extended Data Fig. 9. Post-mating modulation of crop enlargement by Burs and ecdysone

a-a', Classification of crop size upon *rk* downregulation in Ms neurons of starved-refed female flies. Distribution of crop sizes did not significantly change relative to *UAS* and *Gal4* controls in virgin females (**a**). In mated females, the distribution shifted towards smaller crop sizes, relative to *UAS* and *Gal4* controls (**a'**). Ranked data are displayed as percentages. **b-e**, Effect of Burs expression from enteroendocrine cells on crop enlargement in virgin (**b**, **d**) and mated (**c**, **e**) females. Representative crop images of *ad libitum*-fed flies virgin females show that crop size was not visibly changed upon downregulation of *Burs* in Pros-expressing

Europe PMC Funders Author Manuscripts

enteroendocrine cells (**b**) relative to *UAS* (**b'**) and Gal4 (**b'**) controls. In mated females, the distribution shifted towards smaller crop sizes (**c**), relative to *UAS* (**c'**) and *Gal4* (**c″**) controls. Quantifications of crop area of genotypes shown in **b-b″** and **c-c″** are shown in **d** and **e** respectively. **f-h**, Thermogenic activation of *Tkg-Gal4*-positive cells (which include Burs-positive enteroendocrine cells but also a very small subset of neurons outside the PI, not shown) resulted in significant reduction of Ms signal in the cell bodies on PI neurons of virgin females, relative to *UAS* and *Gal4* virgin controls. **f-g″,** Representative images of Ms staining in PI neurons of the genotypes quantified in **h**. Reduction of Ms staining is apparent in PI neurons of virgin females upon activation of *Tkg-Gal4*-positive cells (**f**) relative to *UAS* (**f'**) and *Gal4* (**f″**) virgin controls. The difference between activated (**g**) vs control (**g**', **g** ″) flies was not apparent when female flies were mated (presumably because more Ms peptide has been released in controls). Fluorescence signals are pseudo-coloured; high to low intensity is displayed as warm (yellow) to cold (blue) colours. **i-j**, Effect of gut hormone release from enteroendocrine cells on crop enlargement. Representative crop images of *ad libitum*-fed female flies shows that crop size was increased upon thermogenic activation of *Tkg-Gal4*-positive cells (**i**) relative to *UAS* (**i'**) and *Gal4* (**i″**) controls, quantified in **j**. We note that the *Tkg-Gal4*-positive cells include most Burs-positive enteroendocrine cells as well as a very small subset of central neurons outside the PI (not shown). **k-l**, Effect of ecdysone and Burs signalling in *Taotie* neurons on crop enlargement after mating. Representative crop images of starved-refed mated females show that, relative to the *UAS GD* control (**k**), downregulation of *EcR* (**k'**) or *rk* (**k″**) resulted in visibly smaller crops. Quantifications of crop area of genotypes shown in **k-k″** are shown in **l**. **m**, Schematic summary of key findings. Post-mating increase in circulating levels of Bursicon and Ecdysone signal via their receptors to Ms-neurons, change their neural activity and lead to crop enlargement. Scale bars **f-g″** = 20μm **b-c″, i-i″** = 500 μm and **k-k″** = 1mm. See Supplementary Information for a list of full genotypes, sample sizes and conditions. In all boxplots, line: median; box: 75th-25th percentiles; whiskers: minimum and maximum. All data points are shown. *: 0.05>p>0.01; **: 0.01>p>0.001; ***: p<0.001.

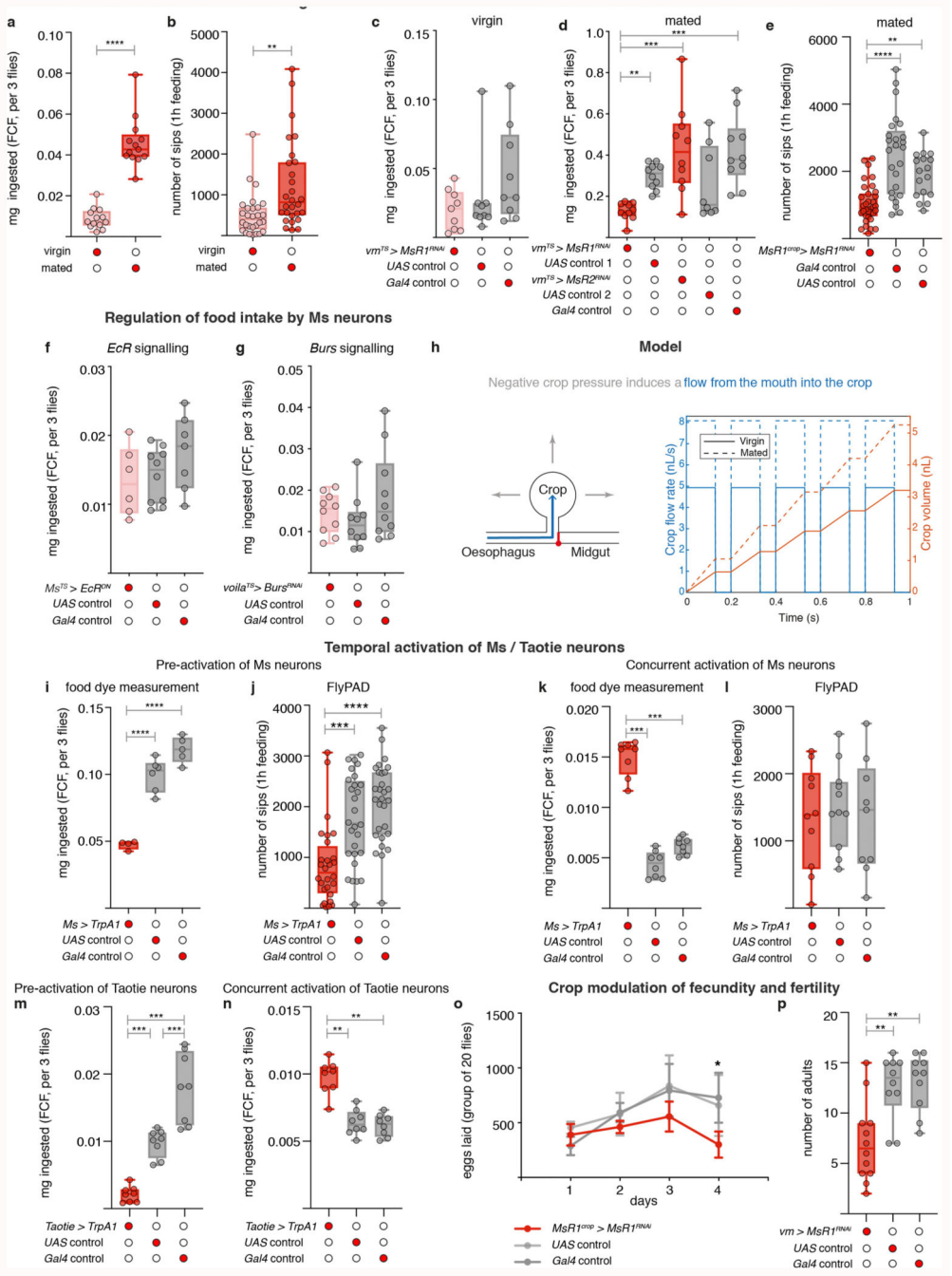

Extended Data Fig. 10. Regulation of food intake, fecundity and fertility by Ms neurons.

a-b, Mated females increase their food intake. Both the amount of ingested dye-laced food (**a**) and the number of sips per fly (**b**) are increased in wild-type mated females relative to virgins. **c-e,** Regulation of food intake by *MsR1* expression in crop muscles. Quantifications of ingested dye show that downregulation of *MsR1* in the visceral muscles of starved-refed virgin females resulted in similar food intake relative to *UAS* and *Gal4* controls (**c**), whereas downregulation of *MsR1*, but not *MsR2*, in mated females, resulted in reduced food intake, relative to *UAS* and *Gal4* controls (**d**). **e**, Quantification of the number of sips per fly show

Europe PMC Funders Author Manuscripts

Europe PMC Funders Author Manuscripts

that downregulation of *MsR1* specifically in crop muscles using an independent driver line also reduced food intake relative to *Gal4* and *UAS* controls in starved-refed mated females. **f**, Quantifications of ingested dye-laced food show that downregulation of *EcR* in Ms neurons of starved-refed virgin females does not significantly affect food intake when compared to *Gal4* and *UAS* controls. **g**, Similarly, quantifications of ingested dye-laced food show that downregulation of *Burs* in Pros-expressing enteroendocrine cells of starved-refed virgin females does not significantly affect food intake when compared to *Gal4* and *UAS* controls (**g**). **h**, In the model, food ingression from the oesophagus is driven by crop enlargement, which is assumed to be linear during sips and constant in between sips. The observed increase in food intake in mated females compared to virgins can be explained by a decrease in negative pressure from -0.8 kPa to -1.3 kPa (increased suction), leading to an increased intake during sips. See Source Data for crop morphometry and FlyPad quantifications used for this crop fluid dynamics model. **i-j**, Thermogenic activation of Ms neurons (*Ms* > *TrpA1*) for 4h prior to the transfer of flies from undyed to dye-laced food reduces the mean amount of ingested dye during the course of 1h (**i**), and reduces the mean number of sips per fly over 1h of feeding (**j**) relative to *Gal4* and *UAS* controls. **k-l**, Concurrent thermogenic activation of Ms neurons during feeding of dye-laced food increases the mean amount of ingested dye during the course of 1h (**k**), but has no effect on the mean number of sips per fly over 1h of feeding (**l'**) relative to *Gal4* and *UAS* controls. **m-n**, Effect of neuronal activation on the regulation of food intake by *Taotie-Gal4*-positive neurons. Quantification of ingested dye-laced food shows that thermogenic activation of Taotie neurons for 4h prior to the switch from undyed to dye-laced food reduced the amount of ingested dye relative to *Gal4* and *UAS* controls over the course of 1h (**m**). By contrast, concurrent activation during feeding of such food increases the amount of ingested dye relative to *Gal4* and *UAS* controls over the course of 1h (**n**). **o**, **p**, Effect of Ms signalling to crop muscles on fecundity and fertility. **o**, Quantification of eggs layed in 24h by mated females shows that *MsR1* downregulation specifically in crop muscles resulted in significantly fewer eggs layed after 4 days relative to *UAS* and *Gal4* controls. **p**, Quantification of adult progeny produced from a 24h period of egg laying by mated females, shows that *MsR1* downregulation in visceral muscles resulted in significantly fewer progeny relative to *UAS* and *Gal4* controls. Sip number measurements were done over 1h of feeding. See Supplementary Information for a list of full genotypes, sample sizes and conditions. In all boxplots, line: median; box: 75th-25th percentiles; whiskers: minimum and maximum. All data points are shown. *: 0.05>p>0.01; **: 0.01>p>0.001; ***: p<0.001.

Supplementary Material

Refer to Web version on PubMed Central for supplementary material.

Acknowledgements

We thank Cyrille Alexandre, Julia Cordero, Alex Gould, Bruno Hudry, Matthias Landgraf, Pierre Léopold, Olena Riabinina, Iris Salecker, Liliane Schoofs, Julie Simpson and Yan Zhu for providing reagents. Sophie Austin and Marion Hartl contributed to the early characterisation of crop innervation. Cyrille Alexandre provided valuable assistance with the *Ms* mutant design. We are grateful to Jake Jacobson and Tatiana Lopes for supporting our work experimentally, and to Guillaume Salbreux for his initial advice on modelling. Chad Whilding assisted with imaging quantifications. Venizelos Papayannopoulos provided valuable comments on the manuscript. This work

was funded by an ERC Advanced Grant and a BBSRC grant to I.M.-A. (ERCAdG 787470 ‘IntraGutSex’ and BB/N000528/1, respectively), and MRC intramural funding to I.M.-A.

Data availability statement

The authors declare that data supporting the findings of this study are available within this manuscript. The datasets generated during and/or analysed during the current study are available from the corresponding author on reasonable request.

References

1. Carvalho GB, Kapahi P, Anderson DJ, Benzer S. Allocrine modulation of feeding behavior by the Sex Peptide of Drosophila. Curr Biol. 2006; 16:692–696. DOI: 10.1016/j.cub.2006.02.064 [PubMed: 16581515]
2. Gittleman JL, Thompson SD. Energy Allocation in Mammalian Reproduction. Amer Zool. 1988; 28:863–875.
3. Johnson ML, Saffrey MJ, Taylor VJ. Gastrointestinal capacity, gut hormones and appetite change during rat pregnancy and lactation. Reproduction. 2019; doi: 10.1530/REP-18-0414
4. Speakman JR. The physiological costs of reproduction in small mammals. Philos Trans R Soc Lond B Biol Sci. 2008; 363:375–398. DOI: 10.1098/rstb.2007.2145 [PubMed: 17686735]
5. Dey S, et al. Cyclic Regulation of Sensory Perception by a Female Hormone Alters Behavior. Cell. 2015; 161:1334–1344. DOI: 10.1016/j.cell.2015.04.052 [PubMed: 26046438]
6. Grunwald Kadow IC. State-dependent plasticity of innate behavior in fruit flies. Curr Opin Neurobiol. 2019; 54:60–65. DOI: 10.1016/j.conb.2018.08.014 [PubMed: 30219668]
7. Krashes MJ, et al. A neural circuit mechanism integrating motivational state with memory expression in Drosophila. Cell. 2009; 139:416–427. DOI: 10.1016/j.cell.2009.08.035 [PubMed: 19837040]
8. Bai L, et al. Genetic Identification of Vagal Sensory Neurons That Control Feeding. Cell. 2019; 179:1129–1143 e1123. DOI: 10.1016/j.cell.2019.10.031 [PubMed: 31730854]
9. Han W, et al. A Neural Circuit for Gut-Induced Reward. Cell. 2018; 175:887–888. DOI: 10.1016/j.cell.2018.10.018 [PubMed: 30340046]
10. Muller PA, et al. Microbiota modulate sympathetic neurons via a gut-brain circuit. Nature. 2020; doi: 10.1038/s41586-020-2474-7
11. Talbot J, et al. Feeding-dependent VIP neuron-ILC3 circuit regulates the intestinal barrier. Nature. 2020; doi: 10.1038/s41586-020-2039-9
12. Tan H-E, et al. The gut–brain axis mediates sugar preference. Nature. 2020; 580:511–516. [PubMed: 32322067]
13. Zimmerman CA, et al. A gut-to-brain signal of fluid osmolarity controls thirst satiation. Nature. 2019; 568:98–102. DOI: 10.1038/s41586-019-1066-x [PubMed: 30918408]
14. Drokhlyansky E, et al. The enteric nervous system of the human and mouse colon at a single-cell resolution. bioRxiv. 2019; doi: 10.1101/746743
15. Kaelberer MM, et al. A gut-brain neural circuit for nutrient sensory transduction. Science. 2018; 361 doi: 10.1126/science.aat5236
16. Lasrado R, et al. Lineage-dependent spatial and functional organization of the mammalian enteric nervous system. Science. 2017; 356:722–726. DOI: 10.1126/science.aam7511 [PubMed: 28522527]
17. Williams EK, et al. Sensory Neurons that Detect Stretch and Nutrients in the Digestive System. Cell. 2016; 166:209–221. DOI: 10.1016/j.cell.2016.05.011 [PubMed: 27238020]
18. Zeisel A, et al. Molecular Architecture of the Mouse Nervous System. Cell. 2018; 174:999–1014 e1022. DOI: 10.1016/j.cell.2018.06.021 [PubMed: 30096314]
19. Miguel-Aliaga I, Jasper H, Lemaitre B. Anatomy and Physiology of the Digestive Tract of Drosophila melanogaster. Genetics. 2018; 210:357–396. DOI: 10.1534/genetics.118.300224 [PubMed: 30287514]

20. Stoffolano JG Jr, Haselton AT. The adult Dipteran crop: a unique and overlooked organ. Annu Rev Entomol. 2013; 58:205–225. DOI: 10.1146/annurev-ento-120811-153653 [PubMed: 23317042]
21. Cao C, Brown MR. Localization of an insulin-like peptide in brains of two flies. Cell Tissue Res. 2001; 304:317–321. [PubMed: 11396725]
22. Cognigni P, Bailey AP, Miguel-Aliaga I. Enteric neurons and systemic signals couple nutritional and reproductive status with intestinal homeostasis. Cell Metab. 2011; 13:92–104. DOI: 10.1016/j.cmet.2010.12.010 [PubMed: 21195352]
23. Rulifson EJ, Kim SK, Nusse R. Ablation of insulin-producing neurons in flies: growth and diabetic phenotypes. Science. 2002; 296:1118–1120. DOI: 10.1126/science.1070058 [PubMed: 12004130]
24. Dus M, et al. Nutrient Sensor in the Brain Directs the Action of the Brain-Gut Axis in Drosophila. Neuron. 2015; 87:139–151. DOI: 10.1016/j.neuron.2015.05.032 [PubMed: 26074004]
25. Kim SK, Rulifson EJ. Conserved mechanisms of glucose sensing and regulation by Drosophila corpora cardiaca cells. Nature. 2004; 431:316–320. DOI: 10.1038/nature02897 [PubMed: 15372035]
26. Lee G, Park JH. Hemolymph sugar homeostasis and starvation-induced hyperactivity affected by genetic manipulations of the adipokinetic hormone-encoding gene in Drosophila melanogaster. Genetics. 2004; 167:311–323. [PubMed: 15166157]
27. Edgecomb RS, Harth CE, Schneiderman AM. Regulation of feeding behavior in adult Drosophila melanogaster varies with feeding regime and nutritional state. J Exp Biol. 1994; 197:215–235. [PubMed: 7852903]
28. McCormick J, Nichols R. Spatial and temporal expression identify dromyosuppressin as a brain-gut peptide in Drosophila melanogaster. J Comp Neurol. 1993; 338:278–288. [PubMed: 8308172]
29. Richer S, Stoffolano JG Jr, Yin CM, Nichols R. Innervation of dromyosuppressin (DMS) immunoreactive processes and effect of DMS and benzethonium chloride on the Phormia regina (Meigen) crop. J Comp Neurol. 2000; 421:136–142. [PubMed: 10813776]
30. Holman GM, Cook BJ, Nachman RJ. Isolation, primary structure and synthesis of leucomyosuppressin, an insect neuropeptide that inhibits spontaneous contractions of the cockroach hindgut. Comparative Biochemistry and Physiology Part C: Comparative Pharmacology. 1986; 85:329–333.
31. Egerod K, et al. Molecular cloning and functional expression of the first two specific insect myosuppressin receptors. Proc Natl Acad Sci U S A. 2003; 100:9808–9813. DOI: 10.1073/pnas.1632197100 [PubMed: 12907701]
32. Harshman LG, Loeb AM, Johnson BA. Ecdysteroid titers in mated and unmated Drosophila melanogaster females. J Insect Physiol. 1999; 45:571–577. [PubMed: 12770342]
33. Schwedes CC, Carney GE. Ecdysone signaling in adult Drosophila melanogaster. J Insect Physiol. 2012; 58:293–302. DOI: 10.1016/j.jinsphys.2012.01.013 [PubMed: 22310011]
34. Reiff T, et al. Endocrine remodelling of the adult intestine sustains reproduction in Drosophila. Elife. 2015; 4:e06930. doi: 10.7554/eLife.06930 [PubMed: 26216039]
35. Scopelliti A, et al. A Neuronal Relay Mediates a Nutrient Responsive Gut/Fat Body Axis Regulating Energy Homeostasis in Adult Drosophila. Cell Metab. 2019; 29:269–284 e210. DOI: 10.1016/j.cmet.2018.09.021 [PubMed: 30344016]
36. Davey KG, Treherne JE. Studies on Crop Function in the Cockroach (Periplaneta Americana L.). J Exp Biol. 1964; 41:513–524.
37. Itskov PM, et al. Automated monitoring and quantitative analysis of feeding behaviour in Drosophila. Nat Commun. 2014; 5:4560. doi: 10.1038/ncomms5560 [PubMed: 25087594]
38. Chapman T, Partridge L. Female fitness in Drosophila melanogaster: an interaction between the effect of nutrition and of encounter rate with males. Proc Biol Sci. 1996; 263:755–759. DOI: 10.1098/rspb.1996.0113 [PubMed: 8763795]
39. Poels J, et al. Myoinhibiting peptides are the ancestral ligands of the promiscuous Drosophila sex peptide receptor. Cell Mol Life Sci. 2010; 67:3511–3522. DOI: 10.1007/s00018-010-0393-8 [PubMed: 20458515]
40. Sieber MH, Spradling AC. Steroid Signaling Establishes a Female Metabolic State and Regulates SREBP to Control Oocyte Lipid Accumulation. Curr Biol. 2015; 25:993–1004. DOI: 10.1016/j.cub.2015.02.019 [PubMed: 25802149]

41. Brunton PJ, Russell JA. The expectant brain: adapting for motherhood. Nat Rev Neurosci. 2008; 9:11–25. DOI: 10.1038/nrn2280 [PubMed: 18073776]
42. Hoekzema E, et al. Pregnancy leads to long-lasting changes in human brain structure. Nat Neurosci. 2017; 20:287–296. DOI: 10.1038/nn.4458 [PubMed: 27991897]
43. Ameku T, Beckwith H, Blackie L, Miguel-Aliaga I. Food, microbes, sex and old age: on the plasticity of gastrointestinal innervation. Curr Opin Neurobiol. 2020; 62:83–91. DOI: 10.1016/j.conb.2019.12.004 [PubMed: 32028080]
44. Hadjieconomou D, et al. Flybow: genetic multicolor cell labeling for neural circuit analysis in Drosophila melanogaster. Nat Methods. 2011; 8:260–266. DOI: 10.1038/nmeth.1567 [PubMed: 21297619]
45. Burke CJ, Waddell S. Remembering nutrient quality of sugar in Drosophila. Curr Biol. 2011; 21:746–750. DOI: 10.1016/j.cub.2011.03.032 [PubMed: 21514159]
46. Fujita M, Tanimura T. Drosophila evaluates and learns the nutritional value of sugars. Curr Biol. 2011; 21:751–755. DOI: 10.1016/j.cub.2011.03.058 [PubMed: 21514154]
47. Ribeiro C, Dickson BJ. Sex peptide receptor and neuronal TOR/S6K signaling modulate nutrient balancing in Drosophila. Curr Biol. 2010; 20:1000–1005. DOI: 10.1016/j.cub.2010.03.061 [PubMed: 20471268]
48. Ikeya T, Galic M, Belawat P, Nairz K, Hafen E. Nutrient-dependent expression of insulin-like peptides from neuroendocrine cells in the CNS contributes to growth regulation in Drosophila. Curr Biol. 2002; 12:1293–1300. [PubMed: 12176357]
49. Miyamoto T, Slone J, Song X, Amrein H. A fructose receptor functions as a nutrient sensor in the Drosophila brain. Cell. 2012; 151:1113–1125. DOI: 10.1016/j.cell.2012.10.024 [PubMed: 23178127]
50. Jenett A, et al. A GAL4-driver line resource for Drosophila neurobiology. Cell Rep. 2012; 2:991–1001. DOI: 10.1016/j.celrep.2012.09.011 [PubMed: 23063364]
51. FlyBase. Asahina, K; Anderson, D, editors. 2013.
52. Tracey WD Jr, Wilson RI, Laurent G, Benzer S. painless, a Drosophila gene essential for nociception. Cell. 2003; 113:261–273. [PubMed: 12705873]
53. Thorne N, Amrein H. Atypical expression of Drosophila gustatory receptor genes in sensory and central neurons. J Comp Neurol. 2008; 506:548–568. DOI: 10.1002/cne.21547 [PubMed: 18067151]
54. de Navas L, Foronda D, Suzanne M, Sanchez-Herrero E. A simple and efficient method to identify replacements of P-lacZ by P-Gal4 lines allows obtaining Gal4 insertions in the bithorax complex of Drosophila. Mech Dev. 2006; 123:860–867. DOI: 10.1016/j.mod.2006.07.010 [PubMed: 16971094]
55. Hudry B, Viala S, Graba Y, Merabet S. Visualization of protein interactions in living Drosophila embryos by the bimolecular fluorescence complementation assay. BMC Biol. 2011; 9:5. doi: 10.1186/1741-7007-9-5 [PubMed: 21276241]
56. Park D, Veenstra JA, Park JH, Taghert PH. Mapping peptidergic cells in Drosophila: where DIMM fits in. PLoS One. 2008; 3:e1896. doi: 10.1371/journal.pone.0001896 [PubMed: 18365028]
57. Zhan YP, Liu L, Zhu Y. Taotie neurons regulate appetite in Drosophila. Nat Commun. 2016; 7:13633. doi: 10.1038/ncomms13633 [PubMed: 27924813]
58. Guo Z, Driver I, Ohlstein B. Injury-induced BMP signaling negatively regulates Drosophila midgut homeostasis. J Cell Biol. 2013; 201:945–961. DOI: 10.1083/jcb.201302049 [PubMed: 23733344]
59. Diao F, Elliott AD, Diao F, Shah S, White BH. Neuromodulatory connectivity defines the structure of a behavioral neural network. Elife. 2017; 6 doi: 10.7554/eLife.29797
60. Balakireva M, Gendre N, Stocker RF, Ferveur JF. The genetic variant Voila causes gustatory defects during Drosophila development. J Neurosci. 2000; 20:3425–3433. [PubMed: 10777805]
61. Song W, Veenstra JA, Perrimon N. Control of lipid metabolism by tachykinin in Drosophila. Cell Rep. 2014; 9:40–47. DOI: 10.1016/j.celrep.2014.08.060 [PubMed: 25263556]
62. McGuire SE, Le PT, Osborn AJ, Matsumoto K, Davis RL. Spatiotemporal rescue of memory dysfunction in Drosophila. Science. 2003; 302:1765–1768. DOI: 10.1126/science.1089035 [PubMed: 14657498]

63. Hudry B, Khadayate S, Miguel-Aliaga I. The sexual identity of adult intestinal stem cells controls organ size and plasticity. Nature. 2016; 530:344–348. DOI: 10.1038/nature16953 [PubMed: 26887495]
64. Nicolai LJ, et al. Genetically encoded dendritic marker sheds light on neuronal connectivity in Drosophila. Proc Natl Acad Sci U S A. 2010; 107:20553–20558. DOI: 10.1073/pnas.1010198107 [PubMed: 21059961]
65. Sugimura K, et al. Distinct developmental modes and lesion-induced reactions of dendrites of two classes of Drosophila sensory neurons. J Neurosci. 2003; 23:3752–3760. [PubMed: 12736346]
66. Hamada FN, et al. An internal thermal sensor controlling temperature preference in Drosophila. Nature. 2008; 454:217–220. DOI: 10.1038/nature07001 [PubMed: 18548007]
67. Baines RA, Uhler JP, Thompson A, Sweeney ST, Bate M. Altered electrical properties in Drosophila neurons developing without synaptic transmission. J Neurosci. 2001; 21:1523–1531. [PubMed: 11222642]
68. Barolo S, et al. A notch-independent activity of suppressor of hairless is required for normal mechanoreceptor physiology. Cell. 2000; 103:957–969. [PubMed: 11136980]
69. Masuyama K, Zhang Y, Rao Y, Wang JW. Mapping neural circuits with activity-dependent nuclear import of a transcription factor. J Neurogenet. 2012; 26:89–102. DOI: 10.3109/01677063.2011.642910 [PubMed: 22236090]
70. Chen TW, et al. Ultrasensitive fluorescent proteins for imaging neuronal activity. Nature. 2013; 499:295–300. DOI: 10.1038/nature12354 [PubMed: 23868258]
71. Sarov M, et al. A genome-wide resource for the analysis of protein localisation in Drosophila. Elife. 2016; 5:e12068. doi: 10.7554/eLife.12068 [PubMed: 26896675]
72. Baena-Lopez LA, Alexandre C, Mitchell A, Pasakarnis L, Vincent JP. Accelerated homologous recombination and subsequent genome modification in Drosophila. Development. 2013; 140:4818–4825. DOI: 10.1242/dev.100933 [PubMed: 24154526]
73. Diao F, et al. Plug-and-play genetic access to drosophila cell types using exchangeable exon cassettes. Cell Rep. 2015; 10:1410–1421. DOI: 10.1016/j.celrep.2015.01.059 [PubMed: 25732830]
74. Eddy SR. Accelerated Profile HMM Searches. PLoS Comput Biol. 2011; 7:e1002195. doi: 10.1371/journal.pcbi.1002195 [PubMed: 22039361]
75. Katoh K, Standley DM. MAFFT multiple sequence alignment software version 7: improvements in performance and usability. Mol Biol Evol. 2013; 30:772–780. DOI: 10.1093/molbev/mst010 [PubMed: 23329690]
76. Capella-Gutierrez S, Silla-Martinez JM, Gabaldon T. trimAl: a tool for automated alignment trimming in large-scale phylogenetic analyses. Bioinformatics. 2009; 25:1972–1973. DOI: 10.1093/bioinformatics/btp348 [PubMed: 19505945]
77. Nguyen LT, Schmidt HA, von Haeseler A, Minh BQ. IQ-TREE: a fast and effective stochastic algorithm for estimating maximum-likelihood phylogenies. Mol Biol Evol. 2015; 32:268–274. DOI: 10.1093/molbev/msu300 [PubMed: 25371430]
78. Peabody NC, et al. Bursicon functions within the Drosophila CNS to modulate wing expansion behavior, hormone secretion, and cell death. J Neurosci. 2008; 28:14379–14391. DOI: 10.1523/JNEUROSCI.2842-08.2008 [PubMed: 19118171]
79. Geminard C, Rulifson EJ, Leopold P. Remote control of insulin secretion by fat cells in Drosophila. Cell Metab. 2009; 10:199–207. DOI: 10.1016/j.cmet.2009.08.002 [PubMed: 19723496]
80. Schoofs L, et al. Isolation, identification, and synthesis of PDVDHFLRFamide (SchistoFLRFamide) in Locusta migratoria and its association with the male accessory glands, the salivary glands, the heart, and the oviduct. Peptides. 1993; 14:409–421. [PubMed: 7687352]
81. Schindelin J, et al. Fiji: an open-source platform for biological-image analysis. Nat Methods. 2012; 9:676–682. DOI: 10.1038/nmeth.2019 [PubMed: 22743772]
82. Adams DC, Otárola-Castillo E. geomorph: an r package for the collection and analysis of geometric morphometric shape data. Methods Ecol Evol. 2013; 4:393–399.

83. Koyama LAJ, et al. Bellymount enables longitudinal, intravital imaging of abdominal organs and the gut microbiota in adult Drosophila. PLoS Biol. 2020; 18:e3000567. doi: 10.1371/journal.pbio.3000567 [PubMed: 31986129]
84. Lopes G, et al. Bonsai: an event-based framework for processing and controlling data streams. Front Neuroinform. 2015; 9:7. doi: 10.3389/fninf.2015.00007 [PubMed: 25904861]
85. Rodriguez A, Ehlenberger DB, Dickstein DL, Hof PR, Wearne SL. Automated three-dimensional detection and shape classification of dendritic spines from fluorescence microscopy images. PLoS One. 2008; 3:e1997. doi: 10.1371/journal.pone.0001997 [PubMed: 18431482]
86. Sejourne J, et al. Mushroom body efferent neurons responsible for aversive olfactory memory retrieval in Drosophila. Nat Neurosci. 2011; 14:903–910. DOI: 10.1038/nn.2846 [PubMed: 21685917]
87. Placais PY, et al. Slow oscillations in two pairs of dopaminergic neurons gate long-term memory formation in Drosophila. Nat Neurosci. 2012; 15:592–599. DOI: 10.1038/nn.3055 [PubMed: 22366756]
88. Buchon N, et al. Morphological and molecular characterization of adult midgut compartmentalization in Drosophila. Cell Rep. 2013; 3:1725–1738. DOI: 10.1016/j.celrep.2013.04.001 [PubMed: 23643535]
89. Leader DP, Krause SA, Pandit A, Davies SA, Dow JAT. FlyAtlas 2: a new version of the Drosophila melanogaster expression atlas with RNA-Seq, miRNA-Seq and sex-specific data. Nucleic Acids Res. 2018; 46:D809–D815. DOI: 10.1093/nar/gkx976 [PubMed: 29069479]

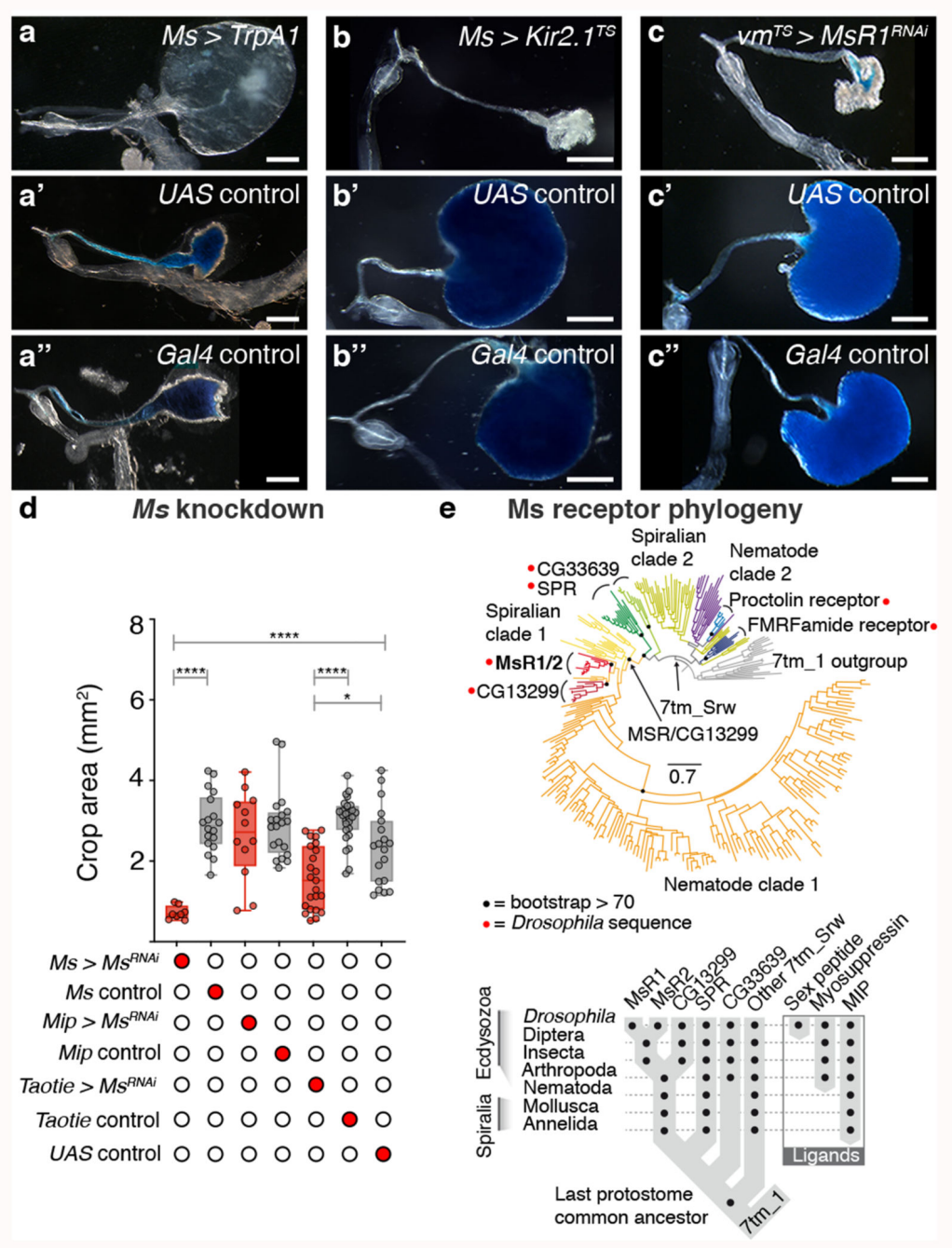

Fig. 1. *Ms/MsR1* regulation of crop enlargement

a-c″, Crop phenotypes resulting from *Ms-Gal4*-driven Ms neuron activation/silencing. *Ms-Gal4*-driven TrpA1 activation enlarges the crop (**a**) compared to controls (**a',a″**). *Ms-Gal4*-driven Kir2.1 silencing (temporally confined with *tub-Gal80^{TS}*) leads to smaller crops (**b**) compared to controls (**b,b″**). *MsR1* downregulation in adult crop muscles (*vm-Gal4*-driven *MsR1-RNAi* expression, temporally confined with *tub-Gal80^{TS}*) leads to smaller crops (**c**), compared to controls (**c',c″**). We note that *vm-Gal4* is expressed in all visceral muscles, but leads to crop muscle-specific downregulation given the neuron- and crop muscle-specific

Europe PMC Funders Author Manuscripts

MsR1 expression, Extended Data Fig. 5a-i'. **d**, *Taotie*-Gal4-driven, but not *Mip-Gal*4-driven *Ms* downregulation significantly reduces crop area (to a lesser degree than Ms neuron silencing, as expected from expression of *Taotie-Gal4* in only a subset of PI Ms neurons, Extended Data 3p-p″). **e**, Myosuppressin receptor phylogeny. Scale bars: **a-c″** = 500μm. In this and all subsequent figures, see Supplementary Information for a list of full genotypes, sample sizes and conditions. Statistics: Kruskal Wallis test. In this and all subsequent boxplots: line: median; box: 75th-25th percentiles; whiskers: minimum and maximum. All data points are shown. *: 0.05>p>0.01; **: 0.01>p>0.001; ***: p<0.001.

Europe PMC Funders Author Manuscripts

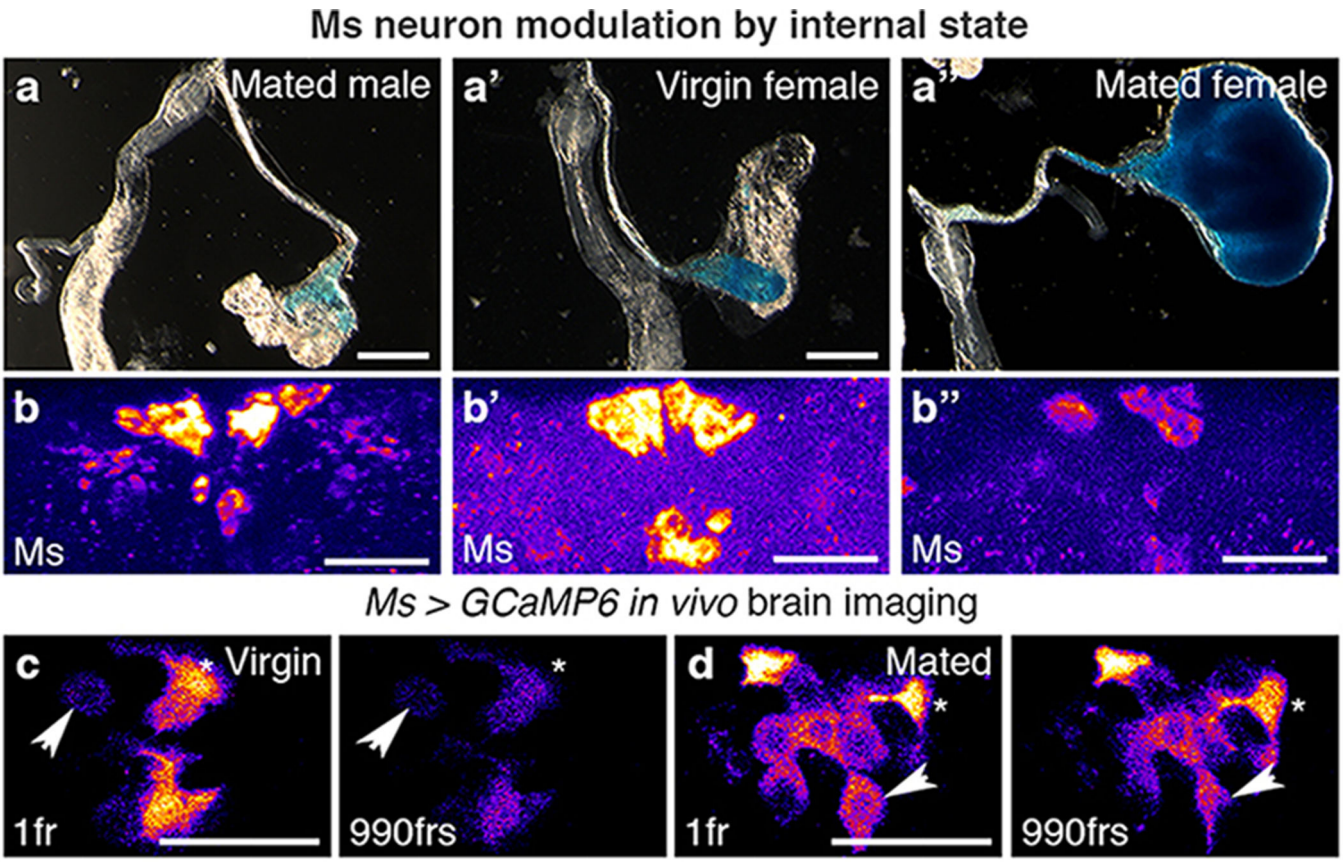

Fig. 2. Reproductive modulation of Ms neurons

a-b″, Representative dissected intestines (top) and Ms stainings of the PI region of the brain (bottom) of wild-type flies. Mated females have more expanded crops (**a″**) and less Ms in their cell bodies (**b″**) than virgin females (**a',b'**) or mated males (**a,b**). In **b-b″**, fluorescence signals are pseudo-coloured; high to low intensity is displayed as warm (yellow) to cold (blue) colours here and thereafter. **c,d**, Temporally defined video snapshots of Ms-driven GCaMP6 activity in the PI of virgin (**c**), or mated (**d**) females, imaged over 1000 frames (frs, each frame acquired every 427 milliseconds). Asterisks and arrows highlight two randomly chosen Ms neurons. Scale bars = 20μm except for **a-a″** = 500μm.

Europe PMC Funders Author Manuscripts

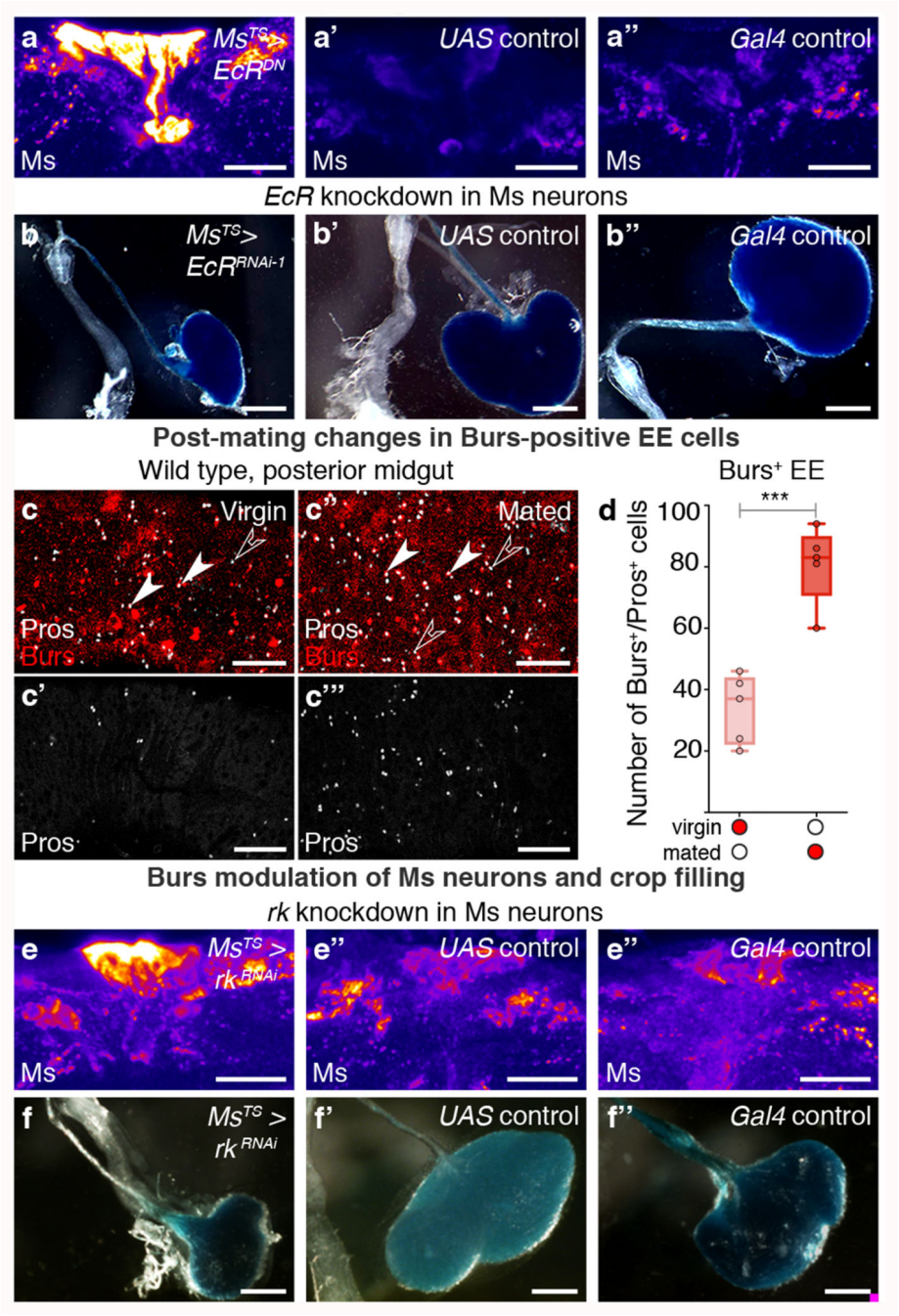

Fig. 3. Steroid and enteroendocrine modulation of Ms neurons and crop enlargement

a-b″, Representative Ms levels (**a-a″**) and crops (**b-b″**) following adult-specific, *Ms-Gal4*-driven expression of EcR^{DN} in mated females. Higher Ms levels in PI Ms neuron cell bodies (**a**) and smaller crops (**b**) are apparent relative to controls (**a',a″,b',b″**). **c'-c‴**, Increased expression of enteroendocrine cell marker Prospero (Pros, in white) and Burs (in red) in the midguts of mated (**c″**,**c‴**) vs virgin (**c**,**c'**) female flies. Filled arrow heads = Pros and Burs-positive cells; empty arrowheads = Pros-positive/Burs-negative cells. **c,c″** are full z projections; **c',c‴** are single z slices. **d**, More Burs-expressing, Pros-positive

enteroendocrine cells are apparent in mated females compared to virgin females. **e-f″**, Representative Ms levels (**e-e″**) and crops (**f-f″**) following adult-specific, *Ms-Gal4*-driven *rk* downregulation in mated females. Higher Ms levels in PI Ms neuron cell bodies (**e**) and smaller crops (**f**) are apparent relative to controls (**e',e″,f',f″**). Scale bars: **a-a″**, **e-e″** = 20μm, **c-c‴** = 50μm and **b-b″, f-f″** = 500μm. Statistics: Mann-Whitney-Wilcoxon test.

Europe PMC Funders Author Manuscripts

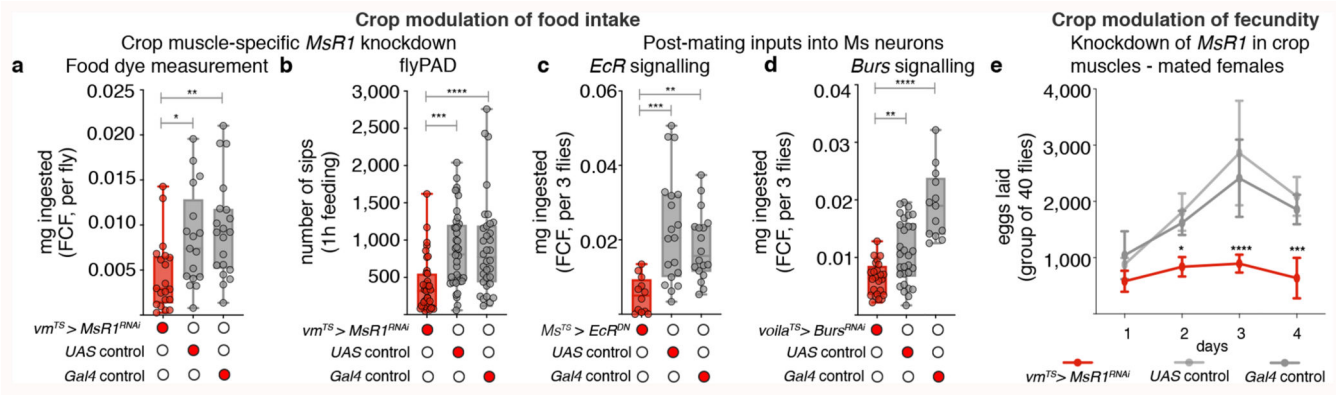

Fig. 4. Post-mating, Ms-mediated crop enlargement increases food intake and reproductive output

a,b, Adult- and crop muscle-specific *MsR1* downregulation. Reduced amount of ingested dye-laced food (**a**) and sips per fly (**b**) are apparent relative to controls. **c,d**, Adult-specific *EcR* downregulation in Ms neurons (**c**) or *Burs* in Pros-expressing enteroendocrine cells (**d**) in mated females. Both result in reduced food ingestion relative to controls. **e**, Reduced Ms signalling to crop muscles reduces fecundity. Data are provided as numbers of eggs laid by mated females per day over the course of 4 days. Adult- and crop muscle-specific *MsR1* downregulation is shown in red and the two genetic controls are shown in grey. Statistics: **a-d,** Kruskal Wallis and **e,** two-way ANOVA followed by a Tukey's multiple comparison test, day and genotype were the 2 independent factors.

Europe PMC Funders Author Manuscripts